Accepted Manuscript

Synthesis and biological evaluation of anthraquinone derivatives as allosteric phosphoglycerate mutase 1 inhibitors for cancer treatment

Ke Huang, Lulu Jiang, Ronghui Liang, Huiti Li, Xiaoxue Ruan, Changliang Shan, Deyong Ye, Lu Zhou

PII: S0223-5234(19)30110-2

DOI: https://doi.org/10.1016/j.ejmech.2019.01.085

Reference: EJMECH 11092

To appear in: *European Journal of Medicinal Chemistry*

Received Date: 7 December 2018

Revised Date: 26 January 2019

Accepted Date: 31 January 2019

Please cite this article as: K. Huang, L. Jiang, R. Liang, H. Li, X. Ruan, C. Shan, D. Ye, L. Zhou, Synthesis and biological evaluation of anthraquinone derivatives as allosteric phosphoglycerate mutase 1 inhibitors for cancer treatment, *European Journal of Medicinal Chemistry* (2019), doi: https://doi.org/10.1016/j.ejmech.2019.01.085.

Synthesis and Biological Evaluation of Anthraquinone Derivatives as Allosteric Phosphoglycerate Mutase 1 Inhibitors for Cancer Treatment

Ke Huang [a,‡], Lulu Jiang [a,‡], Ronghui Liang [b,‡], Huiti Li [a], Xiaoxue Ruan [a], Changliang Shan [b,c*], Deyong Ye [a,*], and Lu Zhou [a,*]

Table of Contents graphic

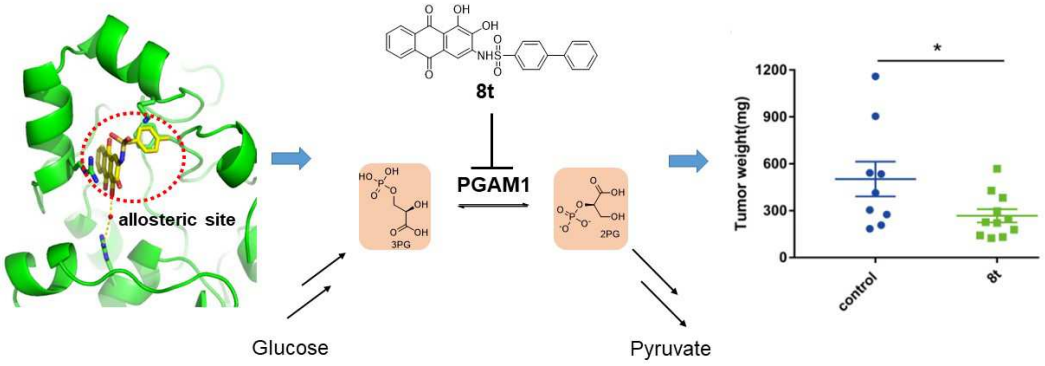

Synthesis and Biological Evaluation of Anthraquinone Derivatives as Allosteric Phosphoglycerate Mutase 1 Inhibitors for Cancer Treatment

Ke Huang [a,‡], Lulu Jiang [a,‡], Ronghui Liang [b,‡], Huiti Li [a], Xiaoxue Ruan [a], Changliang Shan [b,c*], Deyong Ye [a,*], and Lu Zhou [a,*]

[a] Department of Medicinal Chemistry, School of Pharmacy, Fudan University, No. 826, Zhangheng Rd., Shanghai 201203, China

[b]Biomedical Translational Research Institute, Jinan University, Guangzhou, Guangdong 510632, China

[c] State Key Laboratory of Medicinal Chemical Biology, College of Pharmacy, Nankai University, Tianjin 300350, China.

[‡]K.H., L.J. and R.L. contributed to the work equally.

* **Corresponding Author**

email: changliangshan@nankai.edu.cn (C. Shan); dyye@shmu.edu.cn (D. Ye); zhoulu@fudan.edu.cn (L. Zhou).

ABSTRACT

Phosphoglycerate mutase 1 (PGAM1) coordinates glycolysis, pentose phosphate pathway, and serine synthesis to promote tumor growth through the regulation of its substrate 3-phosphoglycerate (**3PG**) and product 2-phosphoglycerate (**2PG**). Herein, based on our previously reported PGAM1 inhibitor **PGMI-004A**, we have developed anthraquinone derivatives as novel allosteric PGAM1 inhibitors and the structure−activity relationship (SAR) was investigated. In addition, we determined the co-crystal structure of PGAM1 and the inhibitor **8g**, demonstrating that the inhibitor was located at a novel allosteric site. Among the derivatives, compound **8t** was selected for further study, with IC_{50} values of 0.25 and approximately 5 μM in enzymatic and cell-based assays, respectively. Mechanistically, compound **8t** reduced the glycolysis and oxygen consumption rate in cancer cells, which led to decreased adenosine 5´-triphosphate (ATP) production and subsequent 5' adenosine monophosphate-activated protein kinase (AMPK) activation. The inhibitor **8t** also exhibited good efficacy in delaying tumor growth in H1299 xenograft model without obvious toxicity. Taken together, this proof-of-principle work further validates PGAM1 as a potential target for cancer therapy and provides useful information on anti-tumor drug discovery targeting PGAM1.

Keywords: Phosphoglycerate mutase 1; Anthraquinone derivatives; Allosteric inhibitors; Cancer treatment

1. INTRODUCTION

Cancer is one of the most lethal diseases and seriously threatens human life worldwide. One of the hallmarks of cancer is the deregulation of cellular energetics [1]. Nearly a century ago, Warburg found that cancer cells prefer anaerobic glycolysis rather than oxidative phosphorylation, whether in anaerobic or aerobic conditions; this was named the "Warburg effect" [2,3]. Although adenosine 5´-triphosphate (ATP) is generated inefficiently in this manner, considerably more glucose is taken in to produce adequate ATP necessary for proliferation [4,5]. More importantly, anaerobic glycolysis provides cancer cells with the building blocks essential for anabolic biosynthesis, such as amino acids and lipids. In addition, through pentose phosphate pathway (PPP), the precursors for nucleotides and the reduced form of nicotinamide adenine dinucleotide phosphate (NADPH), which maintains the cell in an antioxidant status and contributes to lipid synthesis, are generated [5,6].

Despite this knowledge regarding why cancer cells adopt reprogrammed metabolism, the detailed mechanisms remain poorly understood. In recent years there has been an emerging interest in uncovering the secrets of abnormal cancer metabolism and related phenomena [6-10]. Some metabolic enzymes are reported to play pivotal roles in cancer metabolism, including isocitrate dehydrogenase (IDH) [11] and the M2 isozyme of pyruvate kinase (PKM2) [12], to name a few. Since tumor cell metabolism is regarded as cancer's Achilles' heel [6], a trend for targeting cancer metabolism in efforts to develop cancer therapies is growing [13-15]. Small molecules targeting IDH [16,17] and PKM2 [18] as anti-cancer agents have been described, which also illustrates the possibility of regulating cancer cell metabolism to develop cancer treatments.

Phosphoglycerate mutase 1 (PGAM1) is a glycolytic enzyme that catalyzes the conversion of 3-phosphoglycerate (**3PG**) to 2-phosphoglycerate (**2PG**) [19]. Our previous study showed that **3PG** inhibited 6-phosphogluconate dehydrogenase in PPP, while **2PG** activated 3-phosphoglycerate dehydrogenase (PHGDH) in serine synthesis [20]. Inhibition of PGAM1 should give rise to increased intracellular concentration of **3PG** and decreased concentration of **2PG**, which will result in attenuated glycolysis, biosynthesis, and eventually reduced tumor growth [20]. Hence, developing small molecules targeting PGAM1 seems to be "killing two birds with one stone" as a cancer therapeutic strategy [21]. In addition, posttranslational regulation, such as the phosphorylation of Tyr26 by oncogenic signaling [22] and the deacetylation of Lys100 by sirtuin 2 under oxidative stress, stimulate PGAM to promote cancer cell proliferation [23]. Recently, PGAM1 has been reported to facilitate cancer cell migration through the interaction with α-smooth muscle actin (ACTA2) independent of its metabolic activity [24] and promote homologous recombination repair by regulating the deoxyribonucleotide triphosphate nucleoside (dNTP) pool [25]. As well as these diverse roles PGAM1 engages in cancer metabolism, upregulated expression of PGAM1 is observed in multiple tumors, including renal clear cell carcinoma [26], urothelial bladder cancer [27], and pancreatic cancer [28] and it correlates with the prognosis of cancer patients [26-28], which further demonstrates the possibility of targeting PGAM1 for cancer therapy.

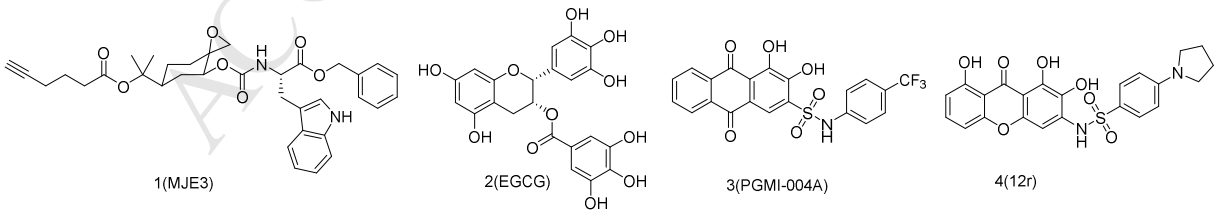

Fig. 1. Representative PGAM1 inhibitors.

In spite of the urge for potent PGAM1 inhibitors, only a few have been reported to date (Figure 1). In 2005, Evans, M.J. et al. identified **MJE3** as a covalent PGAM1 inhibitor by cell-based screening and subsequent in situ proteome reactivity profiling [29]. Later, this group found that **MJE3** labeled PGAM1 on Lys100 by spiroepoxides [30]. Another PGAM1 inhibitor discovered recently is (-)-epigallocatechin-3-gallate (**EGCG**), the major natural catechin from green tea extract, which demonstrated strong molecular potency [31]. Previously, we reported the compounds **PGMI-004A** [20] and xanthone devivative **12r** [32], which inhibited PGAM1 activity with IC_{50} values of 13.1 and 2.7 μM and cancer cell proliferation with IC_{50} values of 25.6 and 5 μM, respectively. Since only a limited amount of anthraquinone analogues were investigated as PGAM1 inhibitors [20], the structure−activity relationship (SAR) of anthraquinone analogues and PGAM1 remains largely unknown. Here we report a series of anthraquinone derivatives targeting PGAM1 as anti-cancer agents and studied the SAR. In addition, we determined the crystal structure of PGAM1 in complex with one of the inhibitors **8g**, which revealed the molecular mechanism of anthraquinone derivatives interacting with PGAM1. The selected compound **8t** adopted the same binding mode as compound **8g** and suppressed glycolysis and induced the generation of reactive oxygen species (ROS) in cancer cells. Finally, we evaluated the pharmacokinetic properties of compound **8t** and it significantly attenuated tumor growth both *in vitro* and *in vivo*.

2. RESULTS AND DISCUSSION

2.1 Synthetic Chemistry

As shown in Scheme 1, we started from commercially available alizarin (**5**). After nitrification of alizarin, followed by reduction with Sn and HCl, the key intermediate **7** was afforded and

sulfonylation of the amino group with a variety of sulfonyl chlorides gave the target compounds **8a-v**. In the meantime, we synthesized compound **9** and further modification of compound **9** via Pd-catalyzed Buchwald-Hartwig cross coupling gave compounds **10a-c**.

Scheme 1. Synthesis of compounds **8a-v**, **10a-c**[a]

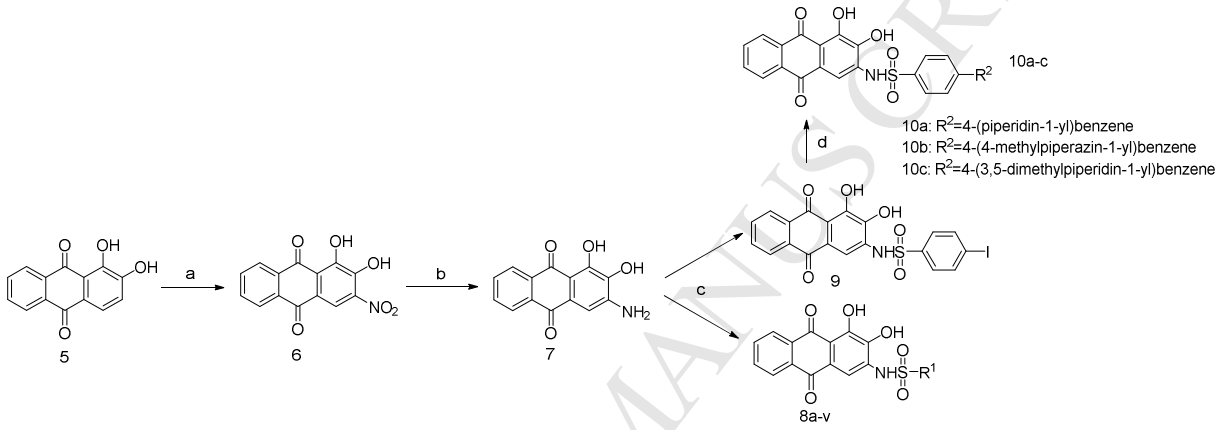

8a: R^1=Me
8b: R^1=$(CH_2)_3CH_3$
8c: R^1=cyclohexane
8d: R^1=NMe_2
8e: R^1=morpholine
8f: R^1=Ph
8g: R^1=4-methylbenzene
8h: R^1=2-thiophene
8i: R^1=5-chloro-2-thiophene
8j: R^1=3-methoxybenzene
8k: R^1=3,4-dimethoxybenzene
8l: R^1=2,4-dimethoxybenzene
8m: R^1=4-fluoro-3-(trifluoromethyl)benzene
8n: R^1=4-chloro-3-(trifluoromethyl)benzene
8o: R^1=4-(*tert*-butyl)benzene
8p: R^1=2-naphthalene
8q: R^1=1-naphthalene
8r: R^1=8-quinoline
8s: R^1=4-(cyclohexyl)benzene
8t: R^1=[1,1'-biphenyl]-4-yl
8u: R^1=4'-fluoro-[1,1'-biphenyl]-4-yl
8v: R^1=4'-chloro-[1,1'-biphenyl]-4-yl

[a]Reagents and conditions: (a) HNO_3, CH_3COOH, 50 °C; (b) Sn, $SnCl_2 \cdot H_2O$, HCl, EtOH; (c) R^3SO_2Cl, Py; (d) $Pd_2(dba)_3$, BINAP, NaOBu-*t*, corresponding amino.

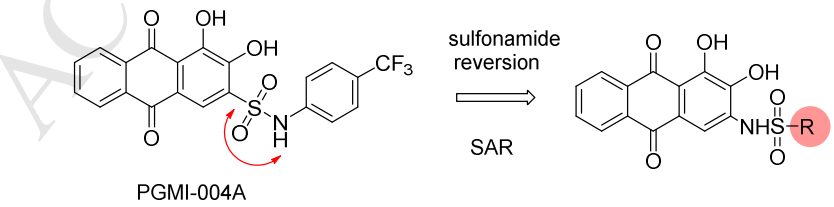

Fig. 2. Design strategy of PGAM1 inhibitors from the lead compound **PGMI-004A** and SAR exploration of the anthraquinone derivatives.

2.2 SAR study of the anthraquinone derivatives

Previously we have discovered that the sulfonamide group of **PGMI-004A** was essential for its biological activity but detailed SAR of anthraquinone derivatives and PGAM1 remained unclear. Here we reversed the sulfonamide group of **PGMI-004A** to investigate the SAR of 3-substituents of the anthraquinone scaffold against PGAM1 (Figure 2). Firstly, we synthesized compounds **8a–i.** As shown in Table 1, compounds containing lipophilic groups, such as cyclohexyl (**8c**) and phenyl (**8f**) were much more potent than compounds containing a hydrophilic group, such as dimethylamino (**8d**) and morpholine (**8e**), suggesting that the substituent at this position lies in a hydrophobic pocket. In addition, introduction of a phenyl group (**8f**) demonstrated better activity than methyl (**8a**) and *n*-butyl (**8b**) groups (Table 1), and methylbenzene (**8g**) performed better than phenyl group (**8f**) (Table 1). Therefore, further modifications of the phenyl ring were explored and compounds **8j–t** were synthesized. The results showed that substitution of bulky moiety, such as cyclohexyl (**8s**) or benzene (**8t**) on the phenyl ring were superior to other substitutions (Table 1). Thus, we synthesized the analogues **8u-v** and **10a-c** that have other bulky groups substituted on the phenyl ring, most of which displayed comparable potency with the inhibitors discussed above (Table 1). However, the hydrophilic substitution of 4-methylpiperazine (**10b**) resulted in sharply reduced potency, which was consistent with the theory proposed above. To this end, the SAR of the anthraquinone derivatives and PGAM1 was investigated, and we have discovered the most potent PGAM1 inhibitor reported to date with an IC_{50} value of 97 nM.

Table 1. Biological activity of compounds **8a-v**, **10a-c**[a]

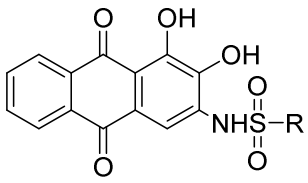

Compd.	R	PGAM1 IC_{50} (μM)	H1299 IC_{50} (μM)	A549 IC_{50} (μM)	PC9 IC_{50} (μM)
8a	CH_3	5.37±0.38	28.5±6	n.d.	n.d.
8b	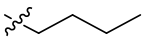	2.05±0.21	38.8±2.0	n.d.	n.d.
8c	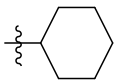	1.75±0.37	21.8±0.4	n.d.	n.d.
8d		>10 μM	n.d.	n.d.	n.d.
8e	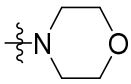	>10 μM	n.d.	n.d.	n.d.
8f	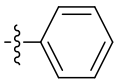	1.50±0.23	21.3±1.1	n.d.	n.d.
8g	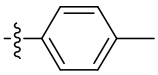	0.36±0.15	7.7±1.0	25.4±1.1	15.7±1.5
8h	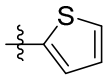	0.84±0.05	25.8±2.6	n.d.	n.d.
8i	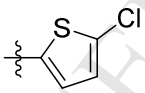	0.55±0.11	17.7±0.2	12.2±2.4	16.1±1.7
8j	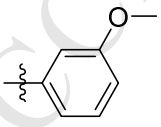	0.48±0.06	27.3±1.4	n.d.	n.d.
8k	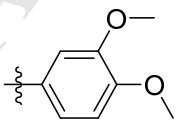	2.81±0.83	26.7±1.5	n.d.	n.d.
8l	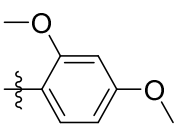	2.86±0.12	20±1	n.d.	n.d.

8m	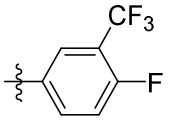	0.63±0.16	22.6±0.3	n.d.	n.d.
8n	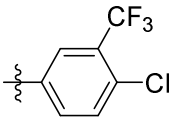	0.55±0.06	13.0±1.2	21.6±0.9	17.5±4.5
8o	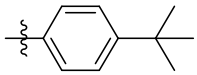	0.49±0.06	10.2±2.2	8.1±0.4	9.5±0.1
8p	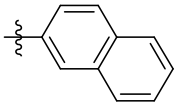	0.19±0.04	8.7±0.5	>100	4.7±2.0
8q	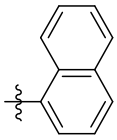	1.29±0.47	7.7±2.1	50.5±0.6	18.1±0.9
8r	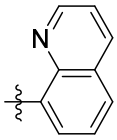	2.05±0.19	47.6±2.8	n.d.	n.d.
8s	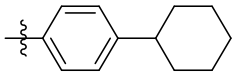	0.097±0.03	4.6±0.8	11.2±1.7	11.5±0.2
8t	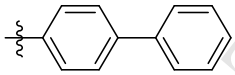	0.25±0.07	6.4±1.3	10.3±0.8	4.8±0.05
8u	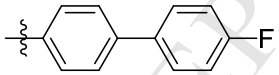	0.26±0.1	6.2±0.2	12.0±0.8	5.4±0.5
8v	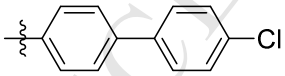	0.14±0.02	6.3±0.5	6.8±0.5	6.6±1.2
10a	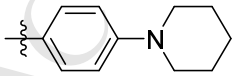	0.33±0.05	10.0±2.5	6.3±0.3	3.0±0.2
10b	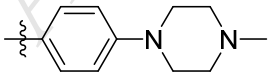	>10 μM	n.d.	n.d.	n.d.
10c	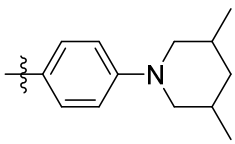	2.6±0.32	10.3±0.7	9.2±2.2	11.6±0.2

cisplatin	n.d.	6.3±0.6	5.6±1.0	2.1±0.3

[a]The data are presented as mean ± s.d.(n=3). n.d. = not determined.

2.3 Binding mode of the anthraquinone inhibitors with PGAM1

To illustrate the binding mode of the anthraquinone inhibitors with PGAM1, we determined the co-crystal structure of PGAM1 with compound **8g** (Table 2). Superposition of pPGAM1-**8g** complex to bisphosphoglycerate mutase (BPGM, a homolog of PGAM1)-**3PG** complex indicated that compound **8g** was located in an allosteric pocket adjacent to the substrate site of **3PG** (Figure 3A). Binding of compound **8g** changed the conformations of the two helixes (99-106, 109-117) near the substrate pocket, stabilizing PGAM1 at an open state. Meanwhile, C terminal residues of PGAM1 (237-255) was not observed in the co-crystal structure, suggesting that C terminus was more flexible owning to the binding with compound **8g** (Figure 3B). Our previous results of molecular dynamics simulation study showed that flexible C-terminal region influenced cofactor binding during the catalytic cycle and induced PGAM1 to the open state [33], which suggested compound **8g** inhibiting PGAM1's enzymatic activity in a similar way. This allosteric pocket is mainly composed of Phe22, Lys100, Arg116, and Arg191 (Figure 3C). In detail, compound **8g** engaged in hydrophobic interactions with the Phe22 of PGAM1 and interacted with the Arg191 through water bridges (Figure 3C). In addition, a π–cation interaction was observed between Arg116 of PGAM1 and the anthraquinone scaffold of compound **8g** (Figure 3C). In the meantime, the co-crystal structure of inactive form of PGAM1 (non—phosphorylated His11) complexed with **8g** was also solved, predicting a dual inhibition despite PGAM1's status (Figure 3D). To validate the binding mode, we constructed mutations of PGAM1 and found that the activity of compound **8g**, and another selected derivative **8t**, toward PGAM1 was impaired to different extents when Phe22, Arg116, and Arg191 were mutated

separately (Figure 3E), which demonstrated that compounds **8g** and **8t** adopted the same binding mode. In addition, analysis by a substrate competitive assay indicated that compound **8t** was a non-competitive inhibitor with **3PG** (Figure 3F), which agreed with the binding mode observed in the crystal structure. In conclusion, the binding mode of the synthesized anthraquinone inhibitors was revealed by co-crystal structures and compound **8t**, was shown to be an allosteric inhibitor non-competitive with the PGAM1 substrate **3PG**.

Table 2. Data collection and refinement statistics

	PGAM1-8g	pPGAM1-8g
Data collection		
Space group	P 2_1 2_1 2_1	P 2_1 2_1 2_1
Cell constants a, b, c (Å)	82.84 85.11 103.05	82.53 82.74 104.36
α, β, γ (°)	90.0, 90.0, 90.0	90.0, 90.0, 90.0
Resolution *(Å)	50-1.99 (2.06-1.99)	50-2.15 (2.23-2.15)
Data completeness (%)	95.3 (100.0)	99.9 (100.0)
No. Observations	320116	282662
No. Unique Reflections	50256	39576
Redundancy	6.7 (7.3)	7.1 (7.3)
R_{merge}	0.17 (0.97)	0.07 (0.74)
$< I/\sigma(I) >^1$	2.19(2.00Å)	3.01(2.16Å)
Refinement		

Resolution (Å)	43.75-1.99 (2.03-1.99)	38.37-2.15 (2.20-2.15)
Data completeness (%)	93.7 (94)	99.7 (97)
No. reflections	47158	39473
R_{work}/R_{free}	0.216/0.244	0.203/0.236
R_{free} test set	2423 (5.11%)	1981 (5.02%)
Wilson B-factor ($Å^2$)	25.9	45.5
F_o,F_c correlation	0.93	0.95
Total number of atoms	4132	3957
Average B, all atoms ($Å^2$)	34.0	47.0
Ligands	MES: 1; KH1: 1; CL: 1;	MES: 1; KH1: 1; CL: 1;
Ramachandran favored (%)	98.5	99.4
Ramachandran allowed (%)	1.5	0.6
Ramachandran outliers (%)	0	0
R.m.s deviations		
Bond lengths (Å)	0.009	0.009
Bond angles(°)	1.202	1.163
PDB accession code	5Y35	5Y64

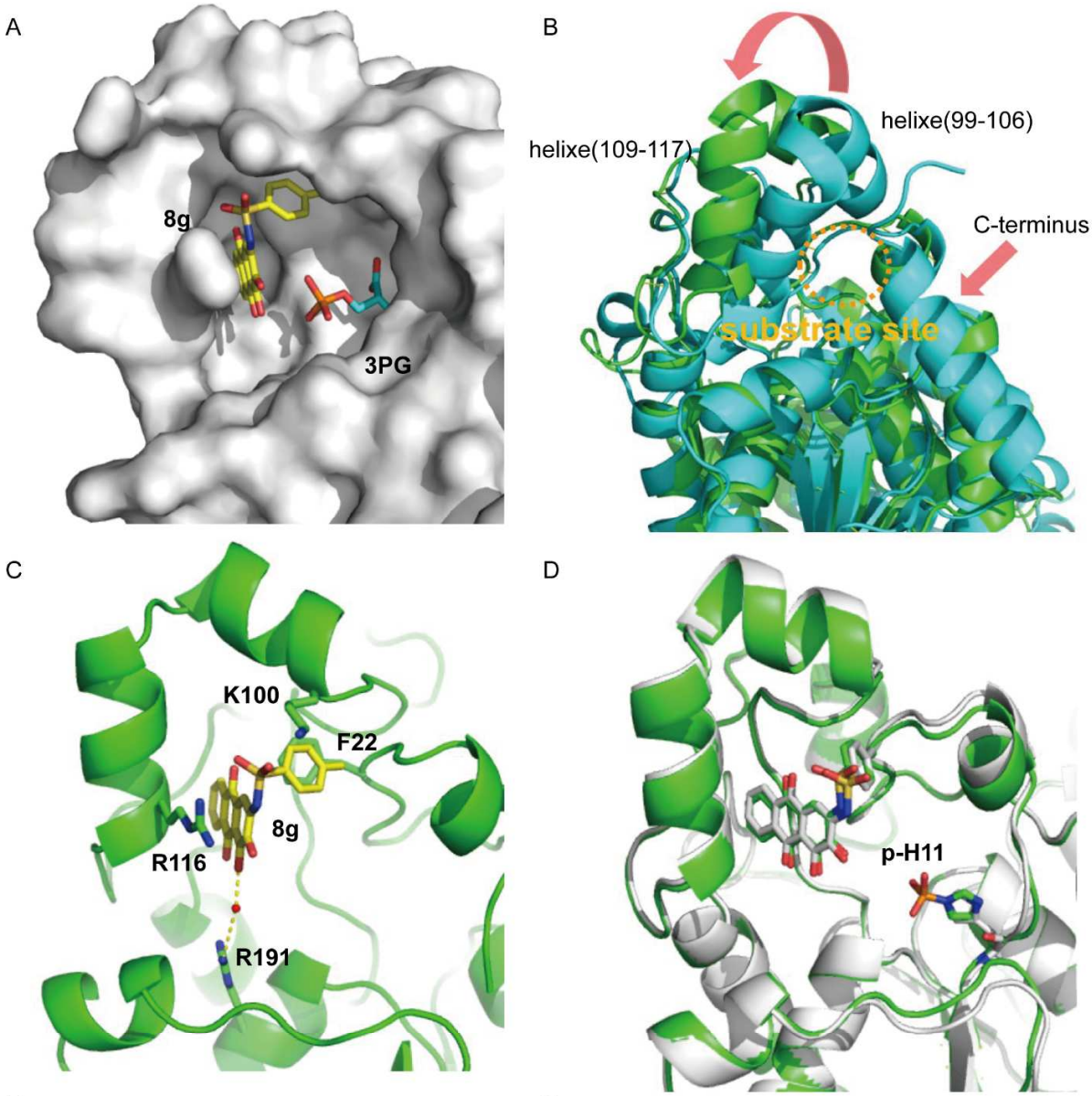
A
8g
3PG
B
helixe(109-117)
helixe(99-106)
C-terminus
substrate site
C
K100
F22
8g
R116
R191
D
p-H11
E
inhibition of PGAM1 activity(%)
100
50
0
8g
8t
WT
F22A
R116H
R191H
F
0μM 8t
0.5μM 8t
2μM 8t
1/V
4
3
2
1
-1
-2
-6
-4
-2
2
4
6
1/[3PG](mM-1)

Fig. 3. Binding mode of the anthraquinone derivatives with PGAM1. (A) Overlay of compound **8g** (PBD: 5Y64) and **3PG** (PBD:2F90) in complex with PGAM1; (B) Superposition of PGAM1(PBD: 5Y64, green) complexed with **8g** and BPGM (PBD:2F90, cyan) complexed with **3PG**; (C) Interactions between compound **8g** and the surrounding residues observed in the co-crystal structure; (D) Structure overlay of non-phosphorylated PGAM1 (PBD: 5Y35, white) and phosphorylated PGAM1 (PBD: 5Y64, green). Active site residue His11 and phosphorylated His11 (p-H11) were shown in sticks. (E) Inhibition of compounds **8g** (5 μM) and **8t** (5 μM) on wild-type and mutated PGAM1; (F) Substrate **3-PG** competitive assay of compound **8t**. The data are presented as mean ± s.e.m.

2.4 Antiproliferative activity of selected inhibitors on cancer cells

We tested the ability of selected compounds, which had IC_{50} values below 10 μM toward PGAM1, to inhibit the proliferation of three cancer cell lines H1299, A549, and PC9 (Table 1). A similar trend in proliferation inhibition was observed as for PGAM1 inhibition, and most of the selected compounds performed similarly in the three different cancer cells. Most of the inhibitors with IC_{50} values above 1 μM toward PGAM1 showed moderate potency toward the cancer cells with IC_{50} values of approximately 20 μM or above. The derivatives that were more potent toward PGAM1 suppressed the proliferation of cancer cells generally more effectively with IC_{50} values ranging from approximately 5–20 μM. Notably, four analogues, **8t**, **8u**, **8v** and **10a**, effectively restrain cancer cell growth with IC_{50} values of approximately 6 μM, while inhibiting PGAM1 with IC_{50} values less than 0.4 μM. Considering the biological activity of these four derivatives on PGAM1 and cancer cells, they were selected for further study.

*2.5 Pharmacokinetic properties of compound **8t** in vivo*

Firstly, we roughly screened the concentrations in the plasma of the four selected compounds, at three different times, post intraperitoneal administration in Institute of Cancer Research (ICR) mice at a dose of 100 mg/kg (Figure S1). The concentrations of compounds **8u**, **8v** and **10a** were much lower than **8t** during the recorded time. Then, we investigated the pharmacokinetic properties of **8t** in detail. After a single intraperitoneal administration of 100 mg/kg in ICR mice, the blood at eight different times was collected and the plasma was analyzed. The results showed that compound **8t** had a half-life of 4.28 h, a high maximum concentration (C_{max}) of 131.01 μg/mL, and an area under the curve ($AUC_{0\text{-}24h}$) of 239.02 μg*h/mL, which indicated a good drug exposure in the blood (Table 3).

Table 3. Pharmacokinetic properties of compound **8t** *in vivo*[a]

$AUC_{0\text{-}24h}$ (μg*h/mL)	$AUC_{0\text{-}inf}$ (μg*h/mL)	CL/F (mL/h)	C_{max} (μg/mL)	T_{max} (h)	V/F (mL)	$t_{1/2}$ (h)
239.02	244.83	11.6	131.01	0.25	71.64	4.28

[a]n = 3 animals per group at every time point. AUC, area under the curve; CL, clearance; F: bioavailability; C_{max}, maximum concentration; T_{max}, time of maximum concentration; V, volume of distribution; $T_{1/2}$, half-life

*2.6 Compound **8t** attenuated tumor growth in vivo safely*

To evaluate the pharmacological efficacy of compound **8t** *in vivo*, we developed H1299 xenograft model by implanting H1299 cells at double flanks subcutaneously in mice. When the average tumor volume reached approximately 200 mm^3, the mice were randomized to be treated with control or compound **8t** at a dose of 100 mg/kg. The tumor volume and the weight of mice were recorded during the test (Figure 4A and Figure 4C). On the day when the mice were

sacrificed, the tumor volumes and tumor weights of the **8t** group were reduced significantly in comparison with the control group (Figure 4A and Figure 4B), with a tolerated weight loss in the mice of approximately 2% (Figure 4C). Additionally, decreased Ki67 staining in the **8t** group further confirmed the anticancer effect *in vivo* (Figure 4D). The kidneys and livers in each group were harvested and no significant difference was observed between the two groups (Figure 4E). Taken as a whole, these results imply that compound **8t** is capable of delaying tumor growth *in vivo* without obvious toxicity.

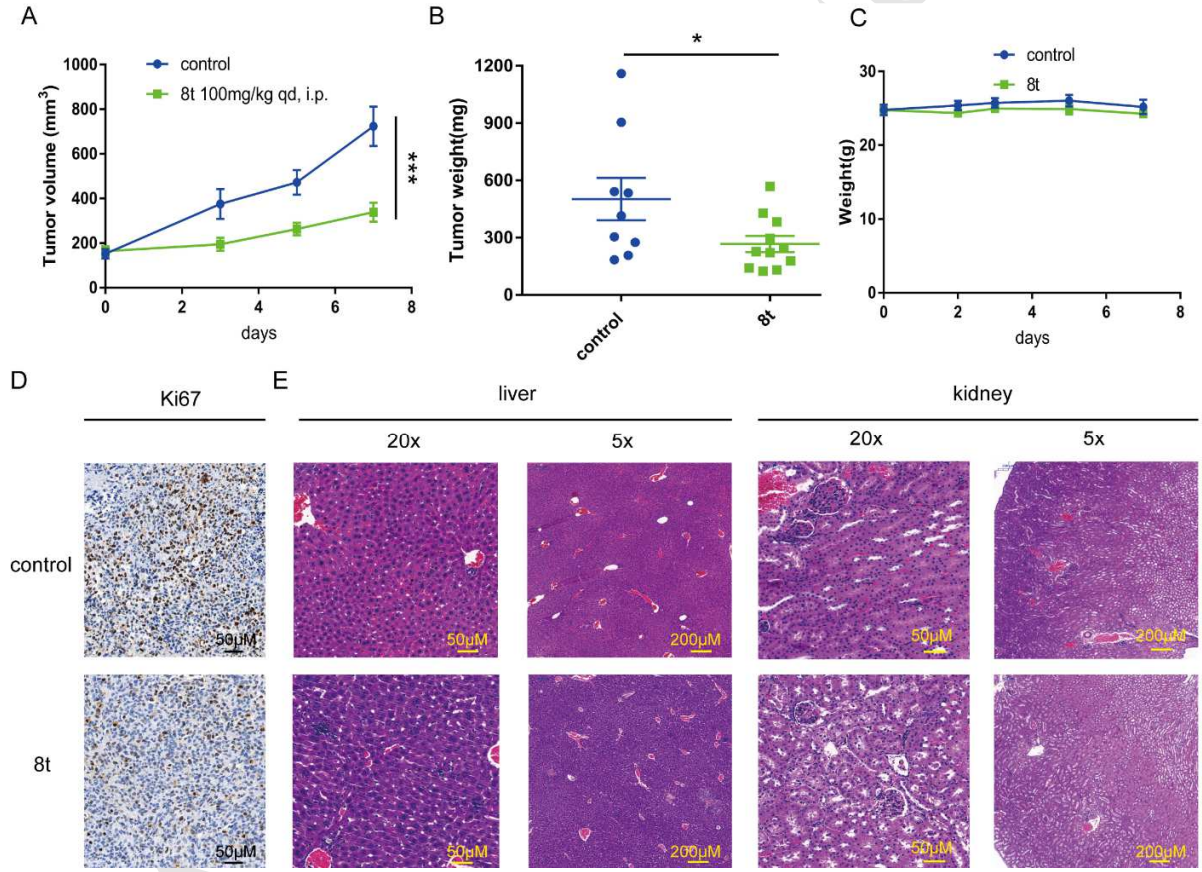

Fig. 4. Compound **8t** attenuated tumor growth in H1299 xenograft model without obvious toxicity. (A) Tumor volumes of control (n = 9/6) and **8t** 100 mg/kg qd, i.p. (n = 11/7) groups during the study. (B) Tumor weights of control and **8t** groups on the last day; (C) The weights of mice in control and **8t** groups; (D) Ki67 staining of the tumor tissues in control and **8t** groups;

(E) Haematoxylin and eosin histology of the kidneys and livers from mice in control and **8t** groups. The data are presented as mean ± s.e.m. and P-values were obtained from the unpaired t-test (*: 0.01 < P < 0.05, **: 0.001 < P < 0.01, ***: 0.0001 < P < 0.001).

*2.7 Compound **8t** reprogramed the Warburg effect*

Considering that PGAM1 plays a vital role in cancer metabolism, we attempted to determine the effect of treatment with the PGAM1 inhibitor **8t** on the Warburg effect in cancer cells. Compound **8t** decreased glycolysis in H1299 cells (Figure 5A), and we further assessed the various parameters of glycolysis function by analyzing the extracellular acidification rate (ECAR) data at several time points. Our results showed that glycolysis, glycolytic capacity, and glycolytic reserve were markedly decreased in a dose dependent manner in H1299 cells treated with compound **8t** (Figure 5A). We also detected real-time oxidative phosphorylation by measuring the cellular oxygen consumption rates (OCR). Our results showed that the OCR were dramatically decreased after H1299 cells were treated with the indicated concentrations of compound **8t** (Figure 5B), suggesting that treatment with compound **8t** led to the inhibition of mitochondrial respiration. We further assessed the various parameters of mitochondrial function by analyzing OCR data at several time points. The data showed that compound **8t** markedly decreased the basal respiration, maximal respiration, and spare capacity in H1299 cells (Figure 5B). Treatment with compound **8t** for 12 h resulted in increased levels of ROS (Figure 6A), but decreased lactate production (Figure 6B) and intracellular ATP levels (Figure 6C). Moreover, treatment with this PGAM1 inhibitor resulted in increased phosphorylation levels of AMPK (Figure 6D) which coordinates cell growth and metabolism [34]. These results suggested that the

selected PGAM1 inhibitor **8t** decreased glycolysis and oxidative phosphorylation which led to decreased ATP level and subsequent AMPK activation in H1299 cells.

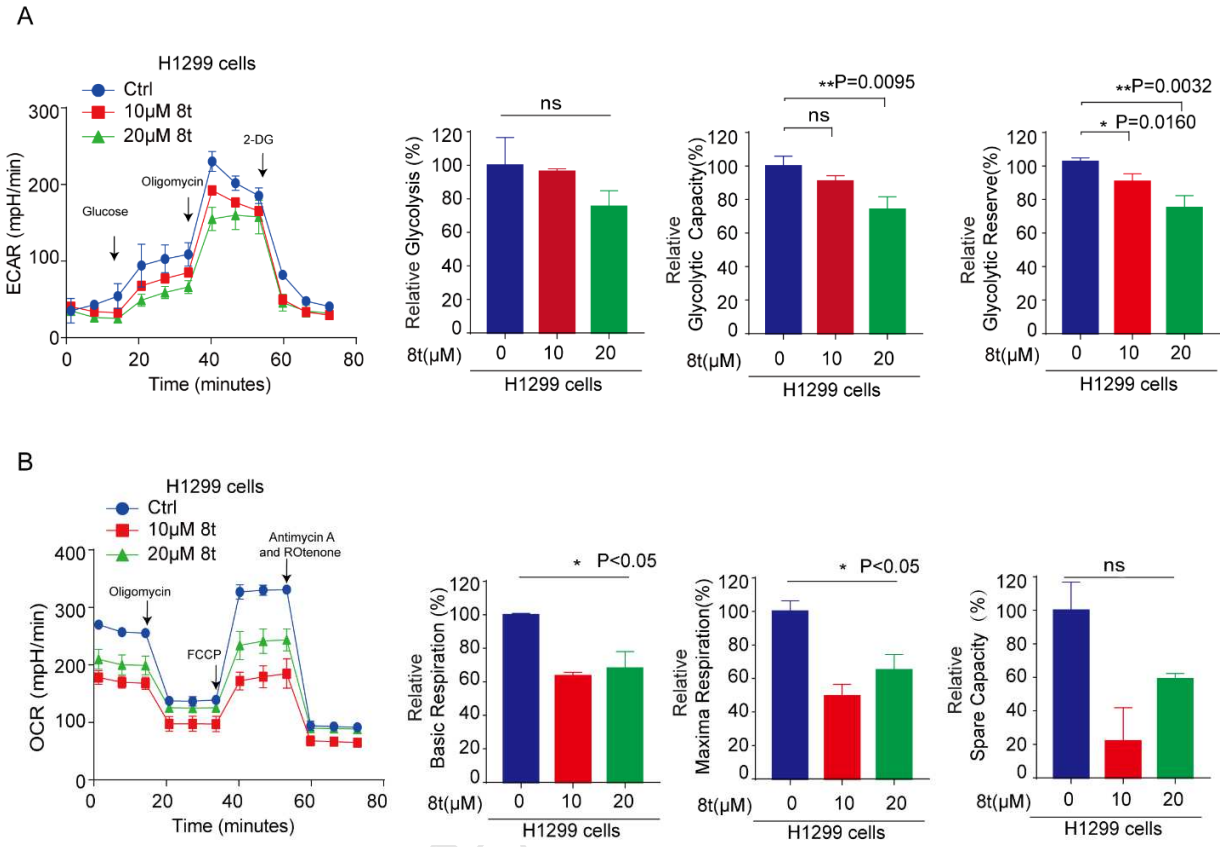

Fig. 5. Compound **8t** decreased the ECAR and OCR. (A) The ECAR (a proxy for the rate of glycolysis) was used to assess the glycolysis using a Seahorse 96XF extracellular flux analyzer following sequential addition of glucose (10 mM), oligomycin (inhibitor of ATP synthase, 1 μM), and 2-deoxyglucose (2-DG, glucose analog, 50 mM), as indicated by the arrows, in H1299 cells in the presence of increasing concentrations of compound **8t.** Data are presented as the mean ± s.d. (ns, not significant, *P < 0.05, **P < 0.01). The representative images represent the mean ECAR ± s.d. of triplicate replicates. (B) H1299 cells were cultured with increasing concentrations of compound **8t**, and the OCR was measured in real time using the Seahorse XF96 Extracellular Flux Analyzer after the basal OCR was measured at three time points,

followed by sequential injection of oligomycin (1 μM), carbonyl cyanide 4-(trifluoromethoxy)phenylhydrazone (FCCP, uncoupler of oxidative phosphorylation, 1 μM), and rotenone/ antimycin A (inhibitor of complex I, III; 0.5 μM). The overall OCR curves were plotted as the mean OCR ± s.d. of triplicate replicates. Basal respiration, maximal respiration, and spare capacity were assessed. Data are presented as the mean ± s.d. (*P < 0.05, **P < 0.01, ***P < 0.001).

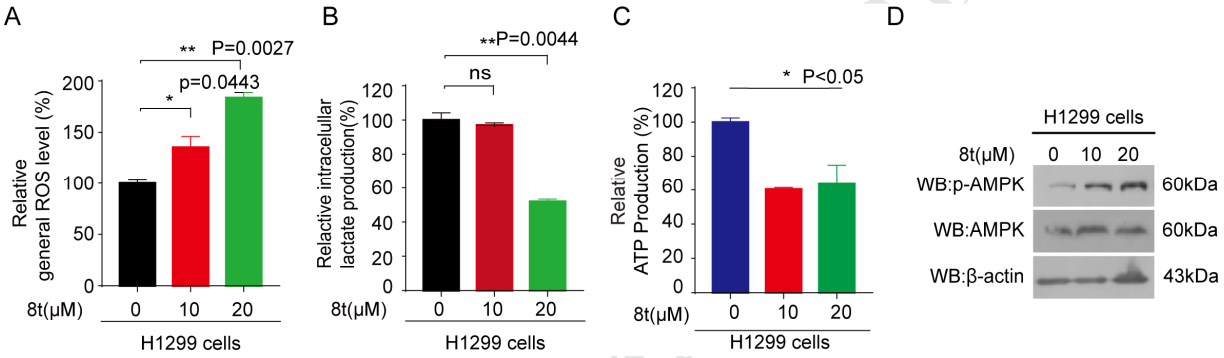

Fig. 6. Compound **8t** increased ROS and decreased lactate and ATP levels, as well as activating AMPK. (A) H1299 cells treated with increasing concentrations of compound **8t** were assayed for general ROS levels. (B) H1299 cells treated with increasing concentrations of compound **8t** were assayed for lactate production. (C) H1299 cells treated with increasing concentrations of compound **8t** were assayed for the levels of ATP, calculated from the OCR. (D) H1299 cells were treated with increasing concentrations of compound **8t**, followed by western blotting to detect the phosphorylation level of AMPK (pT172).

3. CONCLUSIONS

PGAM1 coordinates glycolysis, PPP pathway, and serine synthesis to promote tumor growth, and is thought to be a potential target for cancer therapy. In this study, we focused on the 3-substituents of the anthraquinone scaffold and investigated the SAR of the synthesized

anthraquinone derivatives with regard to PGAM1. Among them, we discovered the most potent PGAM1 inhibitor with IC_{50} value of 97 nM. In addition, we solved the crystal structure of PGAM1 in complex with the inhibitor **8g**, which revealed a novel allosteric site and showed that Phe22, Arg116 and Arg191 are critical residues for binding. These investigations provide a reliable guide for further optimization of anthraquinone derivatives. Furthermore, a competitive assay demonstrated noncompetitive binding of the anthraquinone derivatives with the PGAM1 substrate **3PG**. Compound **8t** demonstrated potent inhibition of PGAM1 and cancer cell proliferation with good pharmacokinetic properties, as well as an ability to alter the Warburg effect and good efficacy in reducing tumor growth *in vivo*. These results illustrate the possibility of targeting PGAM1 for cancer therapy, and compound **8t** is a promising lead compound for further optimization.

4. EXPERIMENTAL SECTION

4.1 Chemistry

All reagents were purchased commercially. Column chromatography was conducted on silica gel (300−400 mesh). ^{1}H NMR and ^{13}C NMR spectra were recorded on Bruker AC400 and Bruker AC600 NMR spectrometer respectively and tetramethylsilane was used as an internal reference. Low-resolution mass spectra were performed on Agilent 6120 Quadrupole mass spectrometer with electrospray ionization (ESI). High-resolution mass spectra were determined on triple TOF 5600^{+} MS/MS system (AB Sciex, Concord, Ontario, Canada) in negative ESI mode. The purity of target compounds was determined by high-performance liquid chromatography (HPLC, Agilent ChemStation 1260, DIKMA Diamonsil Plus C18, 250 × 4.6 mm, 5μm, 25 °C, UV 290 nM). Mobile phase A was water and mobile phase B was methanol

containing 0.1% trifluoroacetic acid. Flow rate was 1mL/min using linear gradients as follow: 0-2 min was 60% B, 2-10 min was from 60% B to 95%B, 10-13 min was 95%B, 13-14 min was from 95%B to 60% B,14-18 min was 60% B. All the biologically tested compounds achieved ≥95% purity.

*4.1.1 General procedure for the synthesis of compounds **8a-v***

Step 1. Nitric acid (1.5mL, 33.33mmol) was added dropwise to the suspension of 1,2-dihydroxyanthracene-9,10-dione (5g, 20.8 mmol) in acetic acid (350 mL) at 50□. Then the mixture was cooled to room temperature and a yellow solid (4.15 g, 70 %) of crude product **6** was obtained by filtration [35].

Step 2. Sn (10.5 g, 341 mmol), $SnCl_2 \cdot 2H_2O$ (12.5 g, 55.4 mmol) and concentrated HCl (50.4 mL, 604.8 mmol) were added to the suspension of crude product **6** (1.75 g, 6.14 mmol) in ethanol (350 mL) and the mixture was stirred at room temperature overnight. After getting rid of part of ethanol under reduced pressure, the residue was poured into water (1 L) and a red solid precipitated. A black solid of crude product **7** (1.41 g, 90 %) was obtained after filtration and being dried under vacuum [35].

Step 3. Corresponding sulfonyl chloride (1.5 mmol) was added to the solution of crude product **7** (255 mg, 1 mmol) in dry pyridine (5 mL) and the mixture was stirred at room temperature for 4h. Then it was added to 10% aqueous HCl (50 mL) and the suspension was extracted with ethyl acetate. The organic phase was washed with brine, dried over anhydrous Na_2SO_4 and filtered. The residue was purified by silica chromatography after removal of ethyl acetate to afford compounds **8a-v**.

*4.1.1.1 N-(3,4-dihydroxy-9,10-dioxo-9,10-dihydroanthracen-2-yl) methanesulfonamide (**8a**)*

Yellow solid, yield 45%.^{1}H NMR (400 MHz, DMSO-d_6) δ 12.68 (brs, 1H), 11.00 (brs, 1H), 9.59 (brs, 1H), 8.28-8.09 (m, 2H), 7.99 – 7.85 (m, 2H), 7.81 (s, 1H), 3.17 (s, 3H). ^{13}C NMR (151 MHz, DMSO) δ 187.75, 180.68, 150.49, 142.37, 135.00, 134.22, 133.32, 132.81, 131.84, 126.79, 126.39, 123.95, 112.97, 112.91, 40.80. MS (ESI) (*m/z*): 332.0 $(M-H)^-$. HRMS (ESI) calcd for $C_{15}H_{11}NO_6S$ $[M-H]^-$: 332.0234; found: 332.0237. Purity 96.9% by HPLC.

*4.1.1.2 N-(3,4-dihydroxy-9,10-dioxo-9,10-dihydroanthracen-2-yl) butane-1-sulfonamide (**8b**)*

Orange solid, 39% yield. ^{1}H NMR (400 MHz, DMSO-d_6) δ 12.68 (brs, 1H), 11.01 (brs, 1H), 9.62 (brs, 1H), 8.24 – 8.13 (m, 2H), 7.97 – 7.86 (m, 2H), 7.82 (s, 1H), 3.23 (t, *J* = 7.6Hz, 2H), 1.72 (p, *J* = 7.6 Hz, 2H), 1.39 (h, *J* = 7.6 Hz, 2H), 0.87 (t, *J* = 7.6 Hz, 3H). ^{13}C NMR (151 MHz, DMSO) δ 187.73, 180.69, 150.47, 142.36, 134.99, 134.21, 133.33, 132.82, 131.88, 126.79, 126.38, 123.89, 113.22, 112.88, 52.12, 25.06, 20.71, 13.44. MS (ESI) (*m/z*): 374.0 $(M-H)^-$. HRMS (ESI) calcd for $C_{18}H_{17}NO_6S$ $[M-H]^-$: 374.0704; found: 374.0707. Purity 98.1% by HPLC.

*4.1.1.3 N-(3,4-dihydroxy-9,10-dioxo-9,10-dihydroanthracen-2-yl) cyclohexanesulfonamide (**8c**)*

Orange solid, 60% yield. ^{1}H NMR (400 MHz, DMSO-d_6) δ 12.71 (brs, 1H), 11.05 (brs, 1H), 9.52 (brs, 1H), 8.25 – 8.12 (m, 2H), 7.96 – 7.89 (m, 2H), 7.86 (s, 1H), 3.10 (tt, *J* = 3.6, 12.0 Hz, 1H), 2.10 (d, *J* = 12.4 Hz, 2H), 1.77 (d, *J* = 12.4 Hz, 2H), 1.60 (d, *J* = 12.0 Hz, 1H), 1.44 (qd, *J* = 3.2, 12.6 Hz, 2H), 1.30 – 1.06 (m, 3H). ^{13}C NMR (151 MHz, DMSO) δ 187.72, 180.74, 150.43, 142.21, 134.98, 134.21, 133.35, 132.84, 132.15, 126.79, 126.38, 123.86, 113.53, 112.85, 60.89, 25.94(2C), 24.72, 24.40(2C). MS (ESI) (*m/z*): 400.0 $(M-H)^-$. HRMS (ESI) calcd for $C_{20}H_{19}NO_6S$ $[M-H]^-$: 400.0860; found: 400.0864. Purity 97.3% by HPLC.

*4.1.1.4 N-(3,4-dihydroxy-9,10-dioxo-9,10-dihydroanthracen-2-yl)-N', N'-dimethyl-4-sulfonamide(**8d**)*

Orange solid, 45% yield. ^{1}H NMR (400 MHz, DMSO-d_6) δ 12.67 (brs, 1H), 10.94 (brs, 1H), 9.67 (brs, 1H), 8.24 – 8.11 (m, 2H), 7.96 – 7.87 (m, 2H), 7.84 (s, 1H), 2.77 (s, 6H). ^{13}C NMR (151 MHz, DMSO) δ 187.69, 180.76, 150.33, 141.73, 134.95, 134.20, 133.35, 132.87, 132.37, 126.78, 126.37, 123.84, 112.99, 112.58, 37.74(2C). MS (ESI) (*m/z*): 361.0 $(M-H)^-$. HRMS (ESI) calcd for $C_{16}H_{14}N_2O_6S$ $[M-H]^-$: 361.0500; found: 361.0503. Purity 99.6% by HPLC.

4.1.1.5 N-(3,4-dihydroxy-9,10-dioxo-9,10-dihydroanthracen-2-yl) morpholine-4-sulfonamide ***(8e)***

Red solid, 49% yield. ^{1}H NMR (400 MHz, DMSO-d_6) δ 12.68 (brs, 1H), 10.99 (brs, 1H), 9.87 (brs, 1H), 8.25 – 8.12 (m, 2H), 7.97 – 7.87 (m, 2H), 7.85 (s, 1H), 3.58 (t, J = 4.6 Hz, 4H), 3.12 (t, J = 4.6 Hz, 4H). ^{13}C NMR (151 MHz, DMSO) δ 187.58, 180.56, 150.20, 142.11, 134.81, 134.05, 133.18, 132.72, 131.75, 126.62, 126.22, 123.59, 113.60, 112.68, 65.25(2C), 45.84(2C). MS (ESI) (*m/z*): 403.0 $(M-H)^-$. HRMS (ESI) calcd for $C_{18}H_{16}N_2O_7S$ $[M-H]^-$: 403.0605; found: 403.0603. Purity 95.0% by HPLC.

*4.1.1.6 N-(3,4-dihydroxy-9,10-dioxo-9,10-dihydroanthracen-2-yl) benzenesulfonamide (**8f**)*

Red solid, 55% yield. ^{1}H NMR (400 MHz, DMSO-d_6) δ 12.58 (brs, 1H), 10.89 (brs, 1H), 10.36 (brs, 1H), 8.21 – 8.09 (m, 2H), 7.97-7.81 (m, 4H), 7.75 (s, 1H), 7.69-7.52 (m, 3H).^{13}C NMR (151 MHz, DMSO) δ 187.70, 180.61, 150.26, 142.34, 140.19, 134.96, 134.20, 133.29, 133.19, 132.82, 131.15, 129.36(2C), 126.76, 126.59(2C), 126.36, 123.72, 112.90, 112.34. MS (ESI) (*m/z*): 394.0 $(M-H)^-$. HRMS (ESI) calcd for $C_{20}H_{13}NO_6S_2$ $[M-H]^-$: 394.0391; found: 394.0388. Purity 98.8% by HPLC.

4.1.1.7 N-(3,4-dihydroxy-9,10-dioxo-9,10-dihydroanthracen-2-yl)-4-methylbenzene sulfonamide ***(8g)***

Orange solid, 50% yield. ^{1}H NMR (400 MHz, DMSO-d_6) δ 12.59 (brs, 1H), 10.90 (brs, 1H), 10.25 (brs, 1H), 8.21 – 8.09 (m, 2H), 7.93 – 7.85 (m, 2H), 7.80 (d, *J* = 8.4 Hz, 2H), 7.76 (s, 1H), 7.40 (d, *J* = 8.0 Hz, 2H), 2.35 (s, 3H).^{13}C NMR (151 MHz, DMSO) δ 187.67, 180.62, 150.23, 143.63, 142.03, 137.29, 134.94, 134.18, 133.27, 132.81, 131.30, 129.78(2C), 126.75, 126.68(2C), 126.34, 123.75, 112.78, 112.02, 20.99. MS (ESI) (*m/z*): 408.0 $(M-H)^-$. HRMS (ESI) calcd for $C_{21}H_{15}NO_6S$ $[M-H]^-$: 408.0547; found: 408.0545.

*4.1.1.8 N-(3,4-dihydroxy-9,10-dioxo-9,10-dihydroanthracen-2-yl) thiophene-2-sulfonamide (**8h**)*

Yellow solid, 50% yield.^{1}H NMR (400 MHz, DMSO-d_6) δ 12.58 (brs, 1H), 10.71 (brs, 2H), 8.23 – 8.08 (m, 2H), 7.96 (d, *J* = 4.8 Hz, 1H), 7.94 – 7.85 (m, 2H), 7.83 (s, 1H), 7.66 (d, *J* = 3.6 Hz, 1H), 7.17 (t, *J* = 4.4 Hz, 1H). ^{13}C NMR (151 MHz, DMSO) δ 187.74, 180.59, 150.32, 142.90, 140.53, 134.98, 134.19, 133.77, 133.28, 132.81, 132.57, 130.77, 127.74, 126.76, 126.37, 123.65, 113.13, 112.98. MS (ESI) (*m/z*): 400.0 $(M-H)^-$. HRMS (ESI) calcd for $C_{18}H_{11}NO_6S_2$ $[M-H]^-$: 399.9955; found: 399.9953. Purity 95.2% by HPLC.

*4.1.1.9 5-Chloro-N-(3,4-dihydroxy-9,10-dioxo-9,10-dihydroanthracen-2-yl) thiophene-2-sulfonamide (**8i**)*

Yellow solid, 52% yield. ^{1}H NMR (400 MHz, DMSO-d_6) δ 12.63 (brs, 1H), 11.00 (brs, 1H), 10.72 (brs, 1H), 8.25 – 8.14 (m, 2H), 7.97 – 7.89 (m, 2H), 7.78 (s, 1H), 7.50 (d, *J* = 4.0 Hz, 1H), 7.25 (d, *J* = 4.0 Hz, 1H). ^{13}C NMR (151 MHz, DMSO) δ 187.87, 180.65, 150.40, 143.66, 139.00, 135.46, 135.07, 134.27, 133.35, 132.88, 132.37, 130.24, 128.02, 126.83, 126.46, 123.71, 113.84, 113.52. MS (ESI) (*m/z*): 433.8$(M-H)^-$. HRMS (ESI) calcd for $C_{18}H_{10}ClNO_6S_2$ $[M-H]^-$: 433.9565; found: 433.9562. Purity 96.5% by HPLC.

*4.1.1.10 N-(3,4-dihydroxy-9,10-dioxo-9,10-dihydroanthracen-2-yl)-3-methoxybenzenesulfonamide (**8j**)*

Orange solid, 51% yield. ^{1}H NMR (400 MHz, DMSO-d_6) δ 12.60 (brs, 1H), 10.96 (brs, 1H), 10.36 (brs, 1H), 8.20 – 8.08 (m, 2H), 7.93 – 7.83 (m, 2H), 7.76 (s, 1H), 7.56 – 7.44 (m, 3H), 7.22 (dt, *J* = 2.0, 8.0 Hz, 1H), 3.81 (s, 3H). ^{13}C NMR (151 MHz, DMSO) δ 187.69, 180.62, 159.37, 150.24, 142.22, 141.38, 134.93, 134.17, 133.27, 132.81, 131.12, 130.53, 126.75, 126.34, 123.73, 119.19, 118.69, 112.88, 112.15, 111.55, 55.59. MS (ESI) (*m/z*): 424.0 $(M-H)^-$. HRMS (ESI) calcd for $C_{21}H_{15}NO_7S$ $[M-H]^-$: 424.0496; found: 424.0501. Purity 97.4% by HPLC.

*4.1.1.11 N-(3,4-dihydroxy-9,10-dioxo-9,10-dihydroanthracen-2-yl)-3,4-dimethoxybenzenesulfonamide (**8k**)*

Red solid, 45% yield. ^{1}H NMR (400 MHz, DMSO-d_6) δ 12.61 (s, 1H), 10.95 (s, 1H), 10.12 (s, 1H), 8.18 – 8.08 (m, 2H), 7.93 – 7.82 (m, 2H), 7.78 (s, 1H), 7.55 – 7.46 (m, 2H), 7.12 (d, *J* = 8.4 Hz, 1H), 3.82 (s, 3H), 3.80 (s, 3H). ^{13}C NMR (151 MHz, DMSO) δ 187.63, 180.65, 152.41, 150.20, 148.58, 141.83, 134.89, 134.15, 133.25, 132.79, 131.48, 131.42, 126.73, 126.31, 123.76, 120.55, 112.68, 111.76, 111.13, 109.61, 55.83, 55.72. MS (ESI) (*m/z*): 454.0 $(M-H)^-$. HRMS (ESI) calcd for $C_{22}H_{17}NO_8S$ $[M-H]^-$: 454.0602; found: 454.0606. Purity 95.0% by HPLC.

*4.1.1.12 N-(3,4-dihydroxy-9,10-dioxo-9,10-dihydroanthracen-2-yl)-2,4-dimethoxybenzenesulfonamide (**8l**)*

Yellow solid, 66% yield. ^{1}H NMR (400 MHz, DMSO-d_6) δ 12.62 (brs, 1H), 11.03 (brs, 1H), 9.11 (brs, 1H), 8.20 – 8.08 (m, 2H), 7.93 – 7.83 (m, 2H), 7.79 (s, 1H), 7.74 (d, *J* = 8.8 Hz, 1H), 6.69 (d, *J* = 2.4 Hz, 1H), 6.63 (dd, *J* = 2.4, 8.8 Hz, 1H), 3.85 (s, 3H), 3.79 (s, 3H). ^{13}C NMR (151 MHz, DMSO) δ 187.62, 180.64, 164.91, 158.12, 150.15, 141.11, 134.88, 134.16, 133.25, 132.82, 131.82, 131.53, 126.73, 126.32, 123.85, 118.65, 112.62, 111.12, 105.15, 99.39, 56.35, 55.82. MS (ESI) (*m/z*): 454.0 $(M-H)^-$. HRMS (ESI) calcd for $C_{22}H_{17}NO_8S$ $[M-H]^-$: 454.0602; found: 454.0605. Purity 95.6% by HPLC.

*4.1.1.13 N-(3,4-dihydroxy-9,10-dioxo-9,10-dihydroanthracen-2-yl)-4-fluoro-3-(trifluoromethyl) benzenesulfonamide (**8m**)*

Yellow solid, 50% yield. ^{1}H NMR (400 MHz, DMSO-d_6) δ 12.60 (brs, 1H), 10.99 (brs, 1H), 10.60 (brs, 1H), 8.29 (dd, *J* = 2.4, 6.8 Hz, 1H), 8.22 – 8.12 (m, 3H), 7.97 – 7.86 (m, 2H), 7.77 (t, *J* = 9.6 Hz, 1H), 7.70 (s, 1H). ^{13}C NMR (151 MHz, DMSO) δ 187.82, 180.54, 161.12(d, J = 261.2 Hz), 150.43, 143.67, 137.31, 135.06, 134.25, 134.07(d, J = 10.6 Hz), 133.28, 132.80, 130.03, 126.80, 126.42, 123.71, 121.75(q, J = 273.3 Hz), 118.83(d, J = 21.1 Hz), 117.66(d, J = 13.6 Hz), 117.44(d, J = 13.6 Hz), 114.08, 113.55. MS (ESI) (*m/z*): 480.0 $(M-H)^-$. HRMS (ESI) calcd for $C_{21}H_{11}F_4NO_6S$ $[M-H]^-$: 480.0170; found: 480.0167. Purity 98.5% by HPLC.

*4.1.1.14 4-Chloro-N-(3,4-dihydroxy-9,10-dioxo-9,10-dihydroanthracen-2-yl)-3-(trifluoromethyl) benzenesulfonamide (**8n**)*

Yellow solid, 71% yield. ^{1}H NMR (400 MHz, DMSO-d_6) δ 12.61 (brs, 1H), 11.02 (brs, 1H), 10.66 (brs, 1H), 8.32 (d, *J* = 2.0 Hz, 1H), 8.22 – 8.12 (m, 2H), 8.09 (dd, *J* = 2.0, 8.4 Hz, 1H), 7.98 (d, *J* = 8.8 Hz, 1H), 7.97 – 7.86 (m, 2H), 7.70 (s, 1H). ^{13}C NMR (151 MHz, DMSO) δ 187.83, 180.53, 150.44, 143.75, 139.87, 135.67, 135.07, 134.25, 133.28, 133.02, 132.80, 132.07, 129.91, 127.51(q, J = 31.7 Hz), 126.80, 126.43, 126.19-126.16 (m), 123.71, 122.06 (q, J = 273.3 Hz), 114.19, 113.60. MS (ESI) (*m/z*): 495.8 $(M-H)^-$. HRMS (ESI) calcd for $C_{21}H_{11}ClF_3NO_6S$ $[M-H]^-$: 495.9875; found: 495.9871. Purity 98.1% by HPLC.

*4.1.1.15 4-(Tert-butyl)-N-(3,4-dihydroxy-9,10-dioxo-9,10-dihydroanthracen-2-yl) benzenesulfonamide (**8o**)*

Orange solid, 65% yield. ^{1}H NMR (400 MHz, DMSO-d_6) δ 12.60 (brs, 1H), 10.93 (brs, 1H), 10.30 (brs, 1H), 8.18 – 8.09 (m, 2H), 7.92 – 7.79 (m, 5H), 7.63 (d, *J* = 8.4 Hz, 2H), 1.26 (s, 9H). ^{13}C NMR (151 MHz, DMSO) δ 187.64, 180.63, 156.22, 150.23, 141.80, 137.44, 134.91, 134.16,

133.26, 132.79, 131.44, 126.73, 126.51(2C), 126.32, 126.23(2C), 123.81, 112.70, 111.64, 34.92, 30.71(3C). MS (ESI) (*m/z*): 450.0 $(M-H)^-$. HRMS (ESI) calcd for $C_{24}H_{21}NO_6S$ $[M-H]^-$: 450.1017; found: 450.1026. Purity 100% by HPLC.

*4.1.1.16 N-(3,4-dihydroxy-9,10-dioxo-9,10-dihydroanthracen-2-yl) naphthalene-2-sulfonamide(**8p**)*

Red solid, 65% yield. ^{1}H NMR (400 MHz, DMSO-d_6) δ 12.54 (brs, 1H), 10.67 (brs, 2H), 8.57 (s, 1H), 8.24 – 7.75 (m, 9H), 7.69 (p, *J* = 7.0 Hz, 2H). ^{13}C NMR (151 MHz, DMSO) δ 187.68, 180.58, 150.25, 142.52, 137.29, 134.92, 134.37, 134.14, 133.26, 132.77, 131.52, 131.09, 129.53, 129.31, 129.08, 127.85, 127.76, 127.71, 126.73, 126.31, 123.71, 122.09, 112.95, 112.67. MS (ESI) (*m/z*): 444.0 $(M-H)^-$. HRMS (ESI) calcd for $C_{24}H_{15}NO_6S$ $[M-H]^-$: 444.0547; found: 444.0560. Purity 99.8% by HPLC.

*4.1.1.17 N-(3,4-dihydroxy-9,10-dioxo-9,10-dihydroanthracen-2-yl) naphthalene-1-sulfonamide(**8q**)*

Yellow solid, 65% yield. ^{1}H NMR (400 MHz, DMSO-d_6) δ 12.55 (brs, 1H), 10.88 (brs, 1H), 10.77 (brs, 1H), 8.84 (d, *J* = 8.4 Hz, 1H), 8.32 – 8.22 (m, 2H), 8.17 – 8.05 (m, 3H), 7.90 – 7.82 (m, 2H), 7.78 – 7.64 (m, 4H). ^{13}C NMR (151 MHz, DMSO) δ 187.55, 180.60, 150.10, 141.90, 135.23, 134.89, 134.59, 134.17, 133.84, 133.24, 132.82, 132.53, 129.18, 128.99, 128.16, 127.45, 127.08, 126.72, 126.32, 124.66, 124.47, 123.68, 112.53, 111.66. MS (ESI) (*m/z*): 444.0 $(M-H)^-$. HRMS (ESI) calcd for $C_{24}H_{15}NO_6S$ $[M-H]^-$: 444.0547; found: 444.0557. Purity 98.1% by HPLC.

*4.1.1.18 N-(3,4-dihydroxy-9,10-dioxo-9,10-dihydroanthracen-2-yl) quinoline-8-sulfonamide (**8r**)*

Red solid, 40% yield. ^{1}H NMR (400 MHz, DMSO-d_6) δ 12.48 (brs, 1H), 11.16 (brs, 1H), 9.48 (brs, 1H), 9.11 (s, 1H), 8.58 (d, *J* = 8.4 Hz, 1H), 8.46 (d, *J* = 7.2 Hz, 1H), 8.34 (d, *J* = 8.0 Hz, 1H), 8.12 (t, *J* = 6.4 Hz, 2H), 7.96 – 7.73 (m, 5H). ^{13}C NMR (151 MHz, DMSO) δ 187.64,

180.60, 151.71, 142.16, 137.39, 134.88, 134.83, 134.64, 134.14, 133.85, 133.23, 132.77, 131.55, 131.32, 128.57, 126.71, 126.30, 125.78, 124.00, 122.96, 112.96, 112.85, 110.33. MS (ESI) (*m/z*): 445.0 $(M-H)^-$. HRMS (ESI) calcd for $C_{23}H_{14}N_2O_6S$ $[M-H]^-$: 445.0500; found: 445.0504. Purity 95.9% by HPLC.

*4.1.1.19 4-Cyclohexyl-N-(3,4-dihydroxy-9,10-dioxo-9,10-dihydroanthracen-2-yl) benzenesulfonamide (**8s**)*

Orange solid, 52% yield. ^{1}H NMR (400 MHz, DMSO-d_6) δ 12.58 (brs, 1H), 10.95 (brs, 1H), 10.37 (brs, 1H), 8.20 – 8.09 (m, 2H), 7.94 – 7.76 (m, 5H), 7.45 (d, *J* = 8.0 Hz, 2H), 2.61 – 2.54 (m, 1H), 1.80 – 1.62 (m, 5H), 1.45 – 1.13 (m, 5H). ^{13}C NMR (151 MHz, DMSO) δ 187.65, 180.63, 153.08, 150.22, 141.86, 137.71, 134.92, 134.17, 133.27, 132.80, 131.44, 127.62(2C), 126.75(3C), 126.33, 123.78, 112.71, 111.72, 43.54, 33.40(2C), 26.11(2C), 25.39. MS (ESI) (*m/z*): 476.0 $(M-H)^-$. HRMS (ESI) calcd for $C_{26}H_{23}NO_6S$ $[M-H]^-$: 476.1173; found: 476.1183. Purity 99.5% by HPLC.

*4.1.1.20 N-(3,4-dihydroxy-9,10-dioxo-9,10-dihydroanthracen-2-yl)-[1,1'-biphenyl]-4-sulfonamide (**8t**)*

Orange solid, 60% yield. ^{1}H NMR (400 MHz, DMSO-d_6) δ 12.59 (brs, 1H), 10.76 (brs, 1H), 10.61 (brs, 1H), 8.21 – 8.09 (m, 2H), 7.99 (d, *J* = 8.4 Hz, 2H), 7.94 – 7.83 (m, 4H), 7.82 (s, 1H), 7.72 (d, *J* = 7.6 Hz, 2H), 7.52 – 7.38 (m, 3H). ^{13}C NMR (151 MHz, DMSO) δ 187.68, 180.62, 150.27, 144.52, 142.22, 138.95, 138.19, 134.94, 134.17, 133.27, 132.80, 131.21, 129.09(2C), 128.62, 127.46(2C), 127.32(2C), 127.07(2C), 126.74, 126.34, 123.78, 112.87, 112.17. MS (ESI) (*m/z*): 470.0 $(M-H)^-$. HRMS (ESI) calcd for $C_{26}H_{17}NO_6S$ $[M-H]^-$: 470.0704; found: 470.0704. Purity 100% by HPLC.

*4.1.1.21 N-(3,4-dihydroxy-9,10-dioxo-9,10-dihydroanthracen-2-yl)-4'-fluoro-[1,1'-biphenyl]-4-sulfonamide (**8u**)*

Orange solid, 53% yield. ^{1}H NMR (400 MHz, DMSO-d_6) δ 12.61 (brs, 1H), 10.97 (brs, 1H), 10.40 (brs, 1H), 8.20 – 8.09 (m, 2H), 8.01 – 7.75 (m, 9H), 7.32 (t, *J* = 8.7 Hz, 2H). ^{13}C NMR (151 MHz, DMSO) δ 187.68, 180.61, 162.50(d, J = 246.1 Hz), 150.27, 143.45, 142.22, 138.91, 134.94, 134.67, 134.18, 133.27, 132.79, 131.15, 129.25(d, J = 9.1Hz), 127.41, 127.33, 126.74, 126.34, 123.78, 115.96(d, J = 9.1Hz), 112.89, 112.17. MS (ESI) (*m/z*): 488.0 $(M-H)^-$. HRMS (ESI) calcd for $C_{26}H_{16}FNO_6S$ $[M-H]^-$:488.0610; found: 488.0613. Purity 98.3% by HPLC.

*4.1.1.22 4'-Chloro-N-(3,4-dihydroxy-9,10-dioxo-9,10-dihydroanthracen-2-yl)-[1,1'-biphenyl]-4-sulfonamide (**8v**)*

Yellow solid, 55% yield. ^{1}H NMR (400 MHz, DMSO-d_6) δ 12.61 (brs, 1H), 10.96 (brs, 1H), 10.42 (brs, 1H), 8.20 – 8.11 (m, 2H), 8.01 – 7.86 (m, 6H), 7.81 (s, 1H), 7.76 (d, *J* = 8.8 Hz, 2H), 7.55 (d, *J* = 8.4 Hz, 2H). ^{13}C NMR (151 MHz, DMSO) δ 187.72, 180.64, 150.30, 143.19, 142.30, 139.27, 137.01, 134.98, 134.22, 133.61, 133.29, 132.81, 131.12, 129.09(2C), 128.90(2C), 127.49(2C), 127.40(2C), 126.77, 126.38, 123.80, 112.94, 112.26. MS (ESI) (*m/z*): 504.0 $(M-H)^-$. HRMS (ESI) calcd for $C_{26}H_{16}ClNO_6S$ $[M-H]^-$: 504.0314; found: 504.0319. Purity 98.2% by HPLC.

*4.1.2 General procedure for the synthesis of compounds **10a-c***

Step1. Compound **9** was synthesized according to the same route of **8a-v**.

Step 2. Compound **9** (52.1 mg, 0.1 mmol), tris(dibenzylideneacetone)dipalladium ($Pd_2(dba)_3$,9.2 mg, 0.01 mmol), 2,2'-bis(diphenylphosphino)-1,1'-binaphthyl (BINAP, 9.3 mg, 0.015 mmol), sodium tert-butoxide (NaOBu-t, 48.1 mg, 0.5 mmol) were added to corresponding amino

(1 mL) under argon atmosphere and the mixture was stirred at 85□ overnight. Then it was cooled to room temperature and added to 10% aqueous HCl (20 mL). The suspension was extracted with ethyl acetate and the organic phase was washed with brine, dried over anhydrous Na_2SO_4 and filtered. The residue was purified by silica chromatography after removal of ethyl acetate to afford compounds **10a-c**.

*4.1.2.1 N-(3,4-dihydroxy-9,10-dioxo-9,10-dihydroanthracen-2-yl)-4-(piperidin-1-yl) benzenesulfonamide (**10a**)*

Orange solid, 68% yield. ^{1}H NMR (400 MHz, DMSO-d_6) δ 8.21 – 8.09 (m, 2H), 7.93 – 7.84 (m, 2H), 7.82 (s, 1H), 7.67 (d, *J* = 8.8 Hz, 2H), 6.98 (d, *J* = 8.8 Hz, 2H), 3.38 (q, *J* = 7.0 Hz, 2H), 1.53 (s, 6H), 1.09 (t, *J* = 7.0 Hz, 2H). ^{13}C NMR (151 MHz, DMSO) δ 187.56, 180.64, 153.39, 150.13, 141.34, 134.86, 134.13, 133.29, 132.83, 132.12, 128.51(2C), 126.71, 126.30, 126.08, 123.70, 113.14(2C), 112.33, 111.05, 64.91, 47.56, 24.79, 23.82, 15.17. MS (ESI) (*m/z*): 477.0 $(M-H)^-$. HRMS (ESI) calcd for $C_{25}H_{22}N_2O_6S$ $[M-H]^-$: 477.1126; found: 477.1131. Purity 98.0% by HPLC.

*4.1.2.2 N-(3,4-dihydroxy-9,10-dioxo-9,10-dihydroanthracen-2-yl)-4-(4-methylpiperazin-1-yl) benzenesulfonamide (**10b**)*

Yellow solid, 42% yield. ^{1}H NMR (400 MHz, DMSO-d_6) δ 10.75 (brs, 2H), 8.21 – 8.08 (m, 2H), 7.95 – 7.84 (m, 2H), 7.80 (s, 1H), 7.75 (d, *J* = 8.4 Hz, 2H), 7.12 (d, *J* = 8.8 Hz, 2H), 3.38 (s, 4H), 3.23 (s, 4H), 2.76 (s, 3H). ^{13}C NMR (151 MHz, DMSO) δ 187.59, 180.68, 152.19, 150.28, 141.60, 134.92, 134.20, 133.27, 132.84, 131.79, 128.70, 128.46(2C), 126.73, 126.35, 123.76, 114.19(2C), 112.52, 111.42, 51.62(2C), 43.85(2C), 41.87. MS (ESI) (*m/z*): 492.0 $(M-H)^-$. HRMS (ESI) calcd for $C_{25}H_{23}N_3O_6S$ $[M-H]^-$: 492.1235; found: 492.1240. Purity 96.9% by HPLC.

*4.1.2.3 N-(3,4-dihydroxy-9,10-dioxo-9,10-dihydroanthracen-2-yl)-4-(3,5-dimethylpiperidin-1-yl) benzenesulfonamide (**10c**)*

Orange solid, 63% yield. ^{1}H NMR (400 MHz, DMSO-d_6) δ 12.61 (brs, 1H), 10.86 (brs, 1H), 9.88 (brs, 1H), 8.22 – 8.10 (m, 2H), 7.95 – 7.85 (m, 2H), 7.82 (s, 1H), 7.65 (d, *J* = 8.8 Hz, 2H), 6.99 (d, *J* = 8.8 Hz, 2H), 3.85 (d, *J* = 12.4 Hz, 2H), 2.29 (t, *J* = 12.2 Hz, 2H), 1.72 (d, *J* = 12.8 Hz, 1H), 1.56 (s, 2H), 1.09 (t, *J* = 7.0 Hz, 1H), 0.85 (d, *J* = 6.4 Hz, 6H). ^{13}C NMR (151 MHz, DMSO) δ 187.58, 180.69, 152.90, 150.13, 141.18, 134.90, 134.19, 133.29, 132.85, 132.07, 128.58(2C), 126.74, 126.33, 125.75, 123.83, 113.03(2C), 112.36, 111.04, 64.91, 53.81, 41.76, 40.05, 29.97, 18.94, 15.17. MS (ESI) (*m/z*): 505.0 $(M-H)^-$. HRMS (ESI) calcd for $C_{27}H_{26}N_2O_6S$ $[M-H]^-$: 505.1439; found: 505.1441. Purity 95.7% by HPLC.

4.2 PGAM1 enzymatic assay

After 1μL inhibitor in dimethyl sulfoxide (DMSO) incubated with 49μL 4.6nM recombinant PGAM1, 50μL enzyme mix containing 3 units/ml enolase (Sigma–Aldrich), 3 units/ml recombinant pyruvate kinase M2 (Sigma–Aldrich), 0.6 units/ml recombinant lactatdehydrogenase (LDH, Sigma–Aldrich), 100 mM Tris-HCl, 100 mM KCl, 5 mM $MgCl_2$, 1 mM adenosine diphosphate (ADP), 0.2 mM the reduced form of nicotinamide adenine dinucleotide (NADH) and 4 mM 3PG was added. PGAM1 activity was measured as the decrease in OD at 340 nm. In addition, we performed a counter screening in which 4mM 2PG was added to 50 μL reaction mix containing the indicated inhibitor, 3 units/ml enolase (Sigma–Aldrich), 3 units/ml recombinant pyruvate kinase M2 (Sigma–Aldrich), 0.6 units/ml recombinant LDH (Sigma–Aldrich), 100 mM Tris-HCl, 100 mM KCl, 5 mM $MgCl_2$, 1 mM ADP and 0.2 mM NADH. The other three enzyme activity was measured as the decrease in OD at 340 nm [20].

4.3 Construction of mutant PGAM1

Wild-type plasmid was gifted from Department of Chemistry and Institute for Biophysical Dynamics, University of Chicago, Chicago. To obtain the plasmid of mutant PGAM1 (F22A), standard molecular biology mutagenesis techniques were utilized to substitute the amino acid code at position 22 from phenylalanine (wt) into alanine (mutant; F22A), and confirmed by standard DNA sequencing methods. R116H and R191H mutants were obtained in a similar way. Mutations were performed using KOD-Plus-Neo polymerase (TOYOBO, #KOD-401). The primers used for the mutation were listed below:

PGAM1 F22A Forward: CTGGAGAACCGCTACAGCGGCTGGTAC

PGAM1 F22A Reverse: GTACCAGCCGCTGTAGCGGTTCTCCAG

PGAM1 K116H Forward: CAGGTGAAGATCTGGCACCGCTCCTATGATGTCC

PGAM1 K116H Reverse: GGACATCATAGGAGCGGTGCCAGATCTTCATCTG

PGAM1 K119H Forward: CATGGCAACAGCCTCCACGGCATTGTCAAGCAT

PGAM1 K119H Reverse: ATGCTTGACAATGCCGTGGAGGCTGTTGCCATG

4.4 Protein purification, crystallization, data collection and structure determination

The *C*-terminal His_6-tagged PGAM1 was expressed and affinity purified using Ni-NTA resin following the reported protocols [22]. The crystals of PGAM1 were obtained via the hanging drop vapor-diffusion method at 16□ in a crystallization buffer containing of 100 mM MES 6.0 and 8% (w/v) PEG3350. To obtain the co-crystal of PGAM1 with compound **8g**, the crystals were soaked in reservoir solution containing 500 μM **8g** for hours. Crystals were then cryo-protected by brief immersion in a mixture of mother liquor: glycerol (76:24) prior to flash-frozen in liquid nitrogen.

Diffraction data were collected at beamline BL17U1, BL18U1 and BL19U1 in Shanghai Synchrotron Radiation Facility (SSRF). The data was processed with HKL2000 [36] and the

structure was solved via molecular replacement in CCP4 [37] using an initial model of PGAM1 derived from PDB entry 4GPZ [22]. The ligand restraints were generated using optimization workbench (eLBOW) in Phenix. Manual rebuilding of the model was carried out using the molecular graphics program COOT [38] according to the electronic density. All the graphs were made by Pymol.

4.5 Cell culture and cell viability assays

The human H1299 cell line was obtained from Guangzhou Jenniobio Biotechnology Co., Ltd. (Guangzhou, China), PC9 and A549 cells were gifted from Deng Jiong's lab in the School of Medicine, Shanghai Jiao Tong University. H1299, PC9 cells were maintained in RPMI-1640 medium and A549 cells were maintained in F-12K medium containing 10% fetal bovine serum (FBS), 100 units/ml of Penicillin and 100μg/ml Streptomycin. In cell viability assays, 2000 H1299 cells, A549 cells or 1000 PC9 cells per well were seeded in 96-well plate and attached for 24h. Then these cells were treated with indicated inhibitor for 72h. After incubation with 0.5mg/mL methylthiazolyldiphenyl-tetrazolium bromide (MTT) for 4h, cell viability was measured as the OD at 570nm.

4.6 Cell metabolism determination

The Seahorse XF96 Extracellular Flux Analyzer (Agilent Technologies, Santa Clara, CA, USA) was used to measure extracellular acidification rate (ECAR) and O_2 consumption rate (OCR) according to the manufacturer's protocol. Briefly, H1299 cells were treated with **8t** (10 and 20μM) or phosphate buffer saline (PBS) alone for 12 hours on a 96-well XF Analyzer plate at 10,000 cells per well. Meanwhile, the calibration plate was incubated at 37 °C, in a non-CO_2 incubator overnight. For the glycolysis stress test, after collecting baseline acidification rate data, cells were sequentially treated with glucose (10 mM), oligomycin (inhibitor of ATP synthase; 1

μM), 2-Deoxy-D-glucose (glucose analog, 50 mM), and the subsequent changes were quantified. To determine total electron transport chain capacity, the cells were sequentially exposed to the following compounds: oligomycin (1 μM), FCCP (uncoupler of OXPHOS; 1 μM), rotenone/ antimycin A (inhibitor of complex I, III; 0.5 μM), and the subsequent changes were quantified. Our experiments included eight OCR and ECAR measurements to create a baseline, followed by the injection of rotenone/ antimycin A. Three OCR and ECAR measurements were then made. Cell number was quantified to normalize the data and plotted as the mean± s.d.

4.7 Lactate production

Cellular lactate production was measured with a colorimetric-based lactate assay kit (MBL), In brief, we seeded cells on a 6 well-plate and incubated at 37 °C for overnight. Media on cells was replaced with phenol red-free RPMI medium without FBS when the cells were 50% confluent. The plate was then incubated for 1 hour at 37 °C. After incubation, 1 mL of media from each well was assessed using the lactate assay kit. Cell numbers were counted by a microscope.

4.8 Intracellular Reactive Oxygen Species (ROS) Production

The amount of intracellular ROS was measured by detecting dichlorodihydrofluorescein, which is the cleavage product of carboxy-H2DCFDA (Invitrogen) by ROS. 2×10^5 cells were seeded in 6-well plate. Twenty-four hours after seeding, cells were washed with PBS and loaded with 12.5 μM carboxy-H2DCFDA for 60 min. The cells were harvested, resuspended in PBS and analyzed using a FACS (BD Biosciences; excitation and emission at 490 and 530 nm, respectively).

4.9 Western blotting

Cells were lysed with lysis buffer (1.5M NaCl, 1M HEPES [pH=7.0], 1%NP40, 0.1M $Na_4P_2O_7$, 0.1M NaF, 0.1M Na_3VO_4, protease inhibitor) on ice for 30 min and then centrifuged at

12,000 rpm for 15 min at 4°C. Protein samples were loaded into 12% SDS-PAGE, then separated by running for different Voltage, and transferred onto PVDF membranes (Millipore). The membranes were blocked with 5 % non-fat milk for 2 hours and then incubated overnight at 4 °C or at room temperature for 2h with the primary antibody and 1 hour at room temperature with secondary antibody. Signals were detected using Luminol substrate solution.

4.10 Pharmacokinetic study in vivo

Compounds **8t, 8u, 8v** and **10a** was formulated in 7% DMSO, 7% Cremophor EL plus 86% PBS (v: v: v) and the formulation was employed in all study in vivo. After a single dose at 100 mg/kg of **8t** were administered intraperitoneally in male ICR mice, 0.1 mL blood samples were collected at 0.25, 0.5, 1, 2, 4, 6, 10, 24h in microtubes containing heparin as anticoagulant. After the blood was centrifugated, the plasma was obtained and extracted with methanol. The supernatant was transferred for HPLC detection after centrifugation at 12,000 rpm for 10 minutes.

*4.11 The HPLC method of quantifying compound **8t***

Compound **8t** was quantified by HPLC using a standard curve. Every sample was injected by Agilent 1100 HPLC system. Mobile phase A was water and mobile phase B was methanol containing 0.1% trifluoroacetic acid. Flow rate was 1ml/min using linear gradients as follow: 0-2 min was 60% B, 2-10 min was from 60% B to 95%B, 10-13 min was 95%B, 13-14 min was from 95%B to 60% B,14-18 min was 60% B. Peak areas of 9aj in every sample were detected and analyzed according to the standard curve.

4.12 H1299 xenograft model

5×10^6 cells suspended in PBS were injected at double flanks subcutaneously in 4 to 6-week-old male nude mice. When the tumors reached about 200mm^3, the mice were randomly assigned

to be treated with control (n=9/6) or 100 mg/kg **8t** intraperitoneally once a day (n=11/7). The body weight was recorded and the volume of the tumor was calculated using the formula (L × W × W) × (π/6) in which L is the major tumor axis and W is the minor tumor axis. At the end of the experiment, the mice were sacrificed, all tumors were harvested and weighed, kidneys and livers were collected for histopathological analysis. After being fixed overnight in 40% formaldehyde (pH 7.4), the samples were dehydrated in ethanol of graded concentrations. The primary antibody of anti-Ki67 (#27309, Proteintech, USA) used in immunohistochemistry (IHC) was diluted in 0.1 M PBS and immunochemical staining were performed as previously described [39].

Declarations of interest: none

ACKNOWLEDGMENT

This work was financially supported by grants from the Chinese National Natural Science Foundation (grant no. 91853206, 21472026, 21877014), the Shanghai Municipal Committee of Science and Technology(14XD1400300), the program for Shanghai Rising Star (15QA1400300), and the open grant of the State Key Laboratory of Bio-organic and Natural Products Chemistry, CAS. Victoria Muir, PhD, from Liwen Bianji, Edanz Group China (www.liwenbianji.cn/ac), edited the English text of a draft of this manuscript.

ABBREVIATIONS

PGAM1, Phosphoglycerate mutase 1; PPP, pentose phosphate pathway; 3PG, 3-phosphoglycerate; 2PG, 2-phosphoglycerate; SAR, structure−activity relationship; ATP, adenosine 5´-triphosphate; AMPK, 5' adenosine monophosphate-activated protein kinase;

NADPH, nucleotide and nicotinamide adenine dinucleotide phosphate reduced; IDH, isocitrate dehydrogenase; PKM2, M2 isozyme of pyruvate kinase; PHGDH, 3-phosphoglycerate dehydrogenase; ACTA2, α-smooth muscle actin; dNTP, deoxyribonucleotide triphosphate nucleoside; EGCG, (-)-Epigallocatechin-3-gallate; BPGM, bisphosphoglycerate mutase; ROS, reactive oxygen species; ICR, Institute of Cancer Research; C_{max}, maximum concentration; AUC, area under the curve; ECAR, extracellular acidification rate; OCR, oxygen consumption rate; ESI, electrospray ionization; HPLC, high-performance liquid chromatography; DMF, *N*,*N*-dimethylformamide; EDCI, *N*-(3-dimethylaminopropyl)-*N'*-ethylcarbodiimide hydrochloride; HOBt, 1-hydroxybenzotriazole; DIPEA, diisopropylethylamine; $Pd_2(dba)_3$, tris(dibenzylideneacetone)dipalladium; BINAP, 2,2'-bis(diphenylphosphino)-1,1'-binaphthyl; NaOBu-t, sodium tert-butoxide; DMSO, dimethyl sulfoxide; LDH, lactatdehydrogenase; ADP, adenosine diphosphate; NADH, the reduced form of nicotinamide adenine dinucleotide; FBS, fetal bovine serum; MTT, methylthiazolyldiphenyl-tetrazolium bromide; PBS, phosphate buffer saline; IHC, immunohistochemistry.

REFERENCES

(1) Hanahan, D.; Weinberg, R.A. Hallmarks of cancer: the next generation. *Cell* **2011**, *144*, 646-674.

(2) Warburg, O.; Posener, K.; Negelein, E. Ueber den stoffwechsel der tumoren. *Biochem.Z.* **1924**, *152*, 319.

(3) Warburg, O. On the origin of cancer cells. *Science* **1956**, *123*, 309-314.

(4) Vander Heiden, M.G.; Cantley, L.C.; Thompson, C.B. Understanding the Warburg effect: the metabolic requirements of cell proliferation. *Science* **2009**, *324*, 1029-1033.

(5) DeBerardinis, R.J.; Lum, J.J.; Hatzivassiliou, G.; Thompson, C.B. The biology of cancer: metabolic reprogramming fuels cell growth and proliferation. *Cell Metab*. **2008**, *7*, 11-20.

(6) Kroemer, G.; Pouyssegur, J. Tumor cell metabolism: cancer's Achilles' heel. *Cancer Cell* **2008**, *13*, 472-482.

(7) Cantor, J.R.; Sabatini, D.M. Cancer cell metabolism: one hallmark, many faces. *Cancer Discov*. **2012**, *2*, 881-898.

(8) DeNicola, G.M.; Cantley, L.C. Cancer's fuel choice: new flavors for a picky eater. *Mol. Cell* **2015**, *60*, 514-523.

(9) Palm, W.; Thompson, C.B. Nutrient acquisition strategies of mammalian cells. *Nature* **2017**, *546*, 234-242.

(10) Vander Heiden, M.G.; DeBerardinis, R.J. Understanding the Intersections between Metabolism and Cancer Biology. *Cell* **2017**, *168*, 657-669.

(11) Dang, L.; White, D.W.; Gross, S.; Bennett, B.D.; Bittinger, M.A.; Driggers, E.M.; Fantin, V.R.; Jang, H.G.; Jin, S.; Keenan, M.C.; Marks, K.M.; Prins, R.M.; Ward, P.S.; Yen, K.E.; Liau, L.M.; Rabinowitz, J.D.; Cantley, L.C.; Thompson, C.B.; Vander Heiden, M.G.; Su, S.M. Cancer-associated IDH1 mutations produce 2-hydroxyglutarate. *Nature* **2009**, *462*, 739-744.

(12) Christofk, H.R.; Vander Heiden, M.G.; Harris, M.H.; Ramanathan, A.; Gerszten, R.E.; Wei, R.; Fleming, M.D.; Schreiber, S.L.; Cantley, L.C. The M2 splice isoform of pyruvate kinase is important for cancer metabolism and tumour growth. *Nature* **2008**, *452*, 230–233.

(13) Vander Heiden, M.G. Targeting cancer metabolism: a therapeutic window opens. *Nat. Rev. Drug Discov.* **2011**, *10*, 671-684.

(14) Schulze, A.; Harris, A.L. How cancer metabolism is tuned for proliferation and vulnerable to disruption. *Nature* **2012**, *491*, 364-373.

(15) Hay, N. Reprogramming glucose metabolism in cancer: can it be exploited for cancer therapy? *Nat. Rev. Cancer* **2016**, *16*, 635-649.

(16) Wang, F.; Travins, J.; DeLaBarre, B.; Penard-Lacronique, V.; Schalm, S.; Hansen, E.; Straley, K.; Kernytsky, A.; Liu, W.; Gliser, C.; Yang, H.; Gross, S.; Artin, E.; Saada, V.; Mylonas, E.; Quivoron, C.; Popovici-Muller, J.; Saunders, J.O.; Salituro, F.G.; Yan, S.; Murray, S.; Wei, W.; Gao, Y.; Dang, L.; Dorsch, M.; Agresta, S.; Schenkein, D.P.; Biller, S.A.; Su, S.M.; de Botton, S.; Yen, K.E. Targeted inhibition of mutant IDH2 in leukemia cells induces cellular differentiation. *Science* **2013**, *340*, 622-626.

(17) Rohle, D.; Popovici-Muller, J.; Palaskas, N.; Turcan, S.; Grommes, C.; Campos, C.; Tsoi, J.; Clark, O.; Oldrini, B.; Komisopoulou, E.; Kunii, K.; Pedraza, A.; Schalm, S.; Silverman, L.; Miller, A.; Wang, F.; Yang, H.; Chen, Y.; Kernytsky, A.; Rosenblum, M.K.; Liu, W.; Biller, S.A.; Su, S.M.; Brennan, C.W.; Chan, T.A.; Graeber, T.G.; Yen, K.E.; Mellinghoff, I.K. An inhibitor of mutant IDH1 delays growth and promotes differentiation of glioma cells. *Science* **2013**, *340*, 626-630.

(18) Anastasiou, D.; Yu, Y.; Israelsen, W.J.; Jiang, J.K.; Boxer, M.B.; Hong, B.S.; Tempel, W.; Dimov, S.; Shen, M.; Jha, A.; Yang, H.; Mattaini, K.R.; Metallo, C.M.; Fiske, B.P.; Courtney, K.D.; Malstrom, S.; Khan, T.M.; Kung, C.; Skoumbourdis, A.P.; Veith, H.; Southall, N.; Walsh, M.J.; Brimacombe, K.R.; Leister, W.; Lunt, S.Y.; Johnson, Z.R.; Yen, K.E.; Kunii, K.; Davidson, S.M.; Christofk, H.R.; Austin, C.P.; Inglese, J.; Harris, M.H.; Asara, J.M.; Stephanopoulos, G.; Salituro, F.G.; Jin, S.; Dang, L.; Auld, D.S.; Park, H.W.; Cantley, L.C.; Thomas, C.J.; Vander Heiden, M.G. Pyruvate kinase M2

activators promote tetramer formation and suppress tumorigenesis. *Nat. Chem. Biol.* **2012**, *8*, 839-847.

(19) Fothergill-Gilmore, L.A.; Watson, H.C. The phosphoglycerate mutases. *Adv. Enzymol. Relat. Areas Mol. Biol.* **1989**, *62*, 227–313.

(20) Hitosugi, T.; Zhou, L.; Elf, S.; Fan, J.; Kang, H.B.; Seo, J.H.; Shan, C.; Dai, Q.; Zhang, L.; Xie, J.; Gu, T.L.; Jin, P.; Alečković, M.; LeRoy, G.; Kang, Y.; Sudderth, J.A.; DeBerardinis, R.J.; Luan, C.H.; Chen, G.Z.; Muller, S.; Shin, D.M.; Owonikoko, T.K.; Lonial, S.; Arellano, M.L.; Khoury, H.J.; Khuri, F.R.; Lee, B.H.; Ye, K.; Boggon, T.J.; Kang, S.; He, C.; Chen, J. Phosphoglycerate mutase 1 coordinates glycolysis and biosynthesis to promote tumor growth. *Cancer Cell* **2012**, *22*, 585-600.

(21) Chaneton, B.; Gottlieb, E. PGAMgnam style: a glycolytic switch controls biosynthesis. *Cancer Cell* **2012**, *22*, 565-566.

(22) Hitosugi, T.; Zhou, L.; Fan, J.; Elf, S.; Zhang, L.; Xie, J.; Wang, Y.; Gu, T.L.; Alečković, M.; LeRoy, G.; Kang, Y.; Kang, H.B.; Seo, J.H.; Shan, C.; Jin, P.; Gong, W.; Lonial, S.; Arellano, M.L.; Khoury, H.J.; Chen, G.Z.; Shin, D.M.; Khuri, F.R.; Boggon, T.J.; Kang, S.; He, C.; Chen, J. Tyr26 phosphorylation of PGAM1 provides a metabolic advantage to tumours by stabilizing the active conformation. *Nat. Commun.* **2013**, *4*, 1790. doi: 10.1038/ncomms2759.

(23) Xu, Y.; Li, F.; Lv, L.; Li, T.; Zhou, X.; Deng, C.X.; Guan, K.L.; Lei, Q.Y.; Xiong, Y. Oxidative stress activates SIRT2 to deacetylate and stimulate phosphoglycerate mutase. *Cancer Res.* **2014**, *74*, 3630-3642.

(24) Zhang, D.; Jin, N.; Sun, W.; Li, X.; Liu, B.; Xie, Z.; Qu, J.; Xu, J.; Yang, X.; Su, Y.; Tang, S.; Han, H.; Chen, D.; Ding, J.; Tan, M.; Huang, M.; Geng, M. Phosphoglycerate

mutase 1 promotes cancer cell migration independent of its metabolic activity. *Oncogene* **2017**, *36*, 2900-2909.

(25) Qu, J.; Sun, W.; Zhong, J.; Lv, H.; Zhu, M.; Xu, J.; Jin, N.; Xie, Z.; Tan, M.; Lin, S.H.; Geng, M.; Ding, J.; Huang, M. Phosphoglycerate mutase 1 regulates dNTP pool and promotes homologous recombination repair in cancer cells. *J. Cell Biol.* **2017**, *216*, 409-424.

(26) Li, C.; Shu, F.; Lei, B.; Lv, D.; Zhang, S.; Mao, X. Expression of PGAM1 in renal clear cell carcinoma and its clinical significance. *Int. J. Clin. Exp. Pathol.* **2015**, *8*, 9410-9415.

(27) Peng, X.C.; Gong, F.M.; Chen, Y.; Qiu, M.; Cheng, K.; Tang, J.; Ge, J.; Chen, N.; Zeng, H.; Liu, J.Y. Proteomics identification of PGAM1 as a potential therapeutic target for urothelial bladder cancer. *J. Proteomics* **2016**, *132*, 85-92.

(28) Liu, X.; Tan, X.; Liu, P.; Wu, Y.; Qian, S.; Zhang, X. Phosphoglycerate mutase 1 (PGAM1) promotes pancreatic ductal adenocarcinoma (PDAC) metastasis by acting as a novel downstream target of the PI3K/Akt/mTOR pathway. *Oncol. Res.* **2018**, *26*, 1123-1131.

(29) Evans, M.J.; Saghatelian, A.; Sorensen, E.J.; Cravatt, B.F. Target discovery in small-molecule cell-based screens by in situ proteome reactivity profiling. *Nat. Biotechnol.* **2005**, *23*, 1303-1307.

(30) Evans, M.J.; Morris, G.M.; Wu, J.; Olson, A.J.; Sorensen, E.J.; Cravatt, B.F. Mechanistic and structural requirements for active site labeling of phosphoglycerate mutase by spiroepoxides. *Mol. Biosyst.* **2007**, *3*, 495-506.

(31) Li, X.; Tang, S.; Wang, Q.Q.; Leung, E.L.; Jin, H.; Huang, Y.; Liu, J.; Geng, M.; Huang, M.; Yuan, S.; Yao, X.J.; Ding, J. Identification of epigallocatechin-3-gallate as an

inhibitor of phosphoglycerate mutase 1. *Front Pharmacol.* **2017**, *8*, 325. doi: 10.3389/fphar.2017.00325.

(32) Wang, P.; Jiang, L.; Cao, Y.; Zhang, X.; Chen, B.; Zhang, S.; Huang, K.; Ye, D.; Zhou, L. Xanthone derivatives as phosphoglycerate mutase 1 inhibitors: Design, synthesis, and biological evaluation. *Bioorg. Med. Chem.* **2018**, *26*, 1961-1970.

(33) Liu, S.E.; Hu, J.C.; Zhang, H.; Xu, P.; Wan, W.; Zheng, M.Y.; Yu, K.Q.; Ding, H.; Jiang, H.L.; Zhou, L.; Luo, C. Conformation and dynamics of the C-terminal region in human phosphoglycerate mutase 1. *Acta. Pharmacol. Sin.* **2017**, *38*, 1673-1682.

(34) Mihaylova, M.M.; Shaw, R.J. The AMPK signalling pathway coordinates cell growth, autophagy and metabolism. *Nat. Cell Biol.* **2011**, *13*, 1016-1023.

(35) Antonello, C.; Uriarte, E.; Palumbo, M. Diethylaminopropionamido-hydroxy-a nthraquinones as potential anticancer agents: synthesis and characterization. *Arch. Pharm.* **1989**, *322*, 541-544.

(36) Otwinowski, Z; Minor, W. Processing of X-ray diffraction data collected in oscillation mode. *Methods Enzymol.* **1997**, *276*, 307-326.

(37) Winn, M.D.; Ballard, C.C.; Cowtan, K.D.; Dodson, E.J.; Emsley, P.; Evans, P.R.; Keegan, R.M.; Krissinel, E.B.; Leslie, A.G.; McCoy, A.; McNicholas, S.J.; Murshudov, G.N.; Pannu, N.S.; Potterton, E.A.; Powell, H.R.; Read, R.J.; Vagin, A.; Wilson, K.S. Overview of the CCP4 suite and current developments. *Acta Crystallogr. D. Biol. Crystallogr.* **2011**, *67*, 235-242.

(38) Emsley, P.; Cowtan, K. Coot: model-building tools for molecular graphics. *Acta Crystallogr. D. Biol. Crystallogr.* **2004**, *60*, 2126-2132.

(39) Zhu, Y.; Shi, M.; Chen, H.; Gu, J.; Zhang, J.; Shen, B.; Deng, X.; Xie, J.; Zhan, X.; Peng, C. NPM1 activates metabolic changes by inhibiting FBP1 while promoting the tumorigenicity of pancreatic cancer cells. *Oncotarget* **2015**, *6*, 21443-21451.

Synthesis and Biological Evaluation of Anthraquinone Derivatives as Allosteric Phosphoglycerate mutase 1 Inhibitors for Cancer Treatment

Ke Huang [a,‡], Lulu Jiang [a,‡], Ronghui Liang [b,‡], Huiti Li [a], Xiaoxue Ruan [a], Changliang Shan [b,c*], Deyong Ye [a,*], and Lu Zhou [a,*]

Highlights:

- A series of anthraquinone derivatives were synthesized and characterized.
- **8s** was most potent PGAM1 inhibitor reported to date with an IC_{50} value of 97 nM.
- The first co-crystal structure of PGAM1 and its inhibitor revealing a novel allosteric site.
- **8t** effectively inhibited tumor growth both *in vitro* and *in vivo*.